PCCP

Accepted Manuscript

This is an *Accepted Manuscript*, which has been through the Royal Society of Chemistry peer review process and has been accepted for publication.

Accepted Manuscripts are published online shortly after acceptance, before technical editing, formatting and proof reading. Using this free service, authors can make their results available to the community, in citable form, before we publish the edited article. We will replace this *Accepted Manuscript* with the edited and formatted *Advance Article* as soon as it is available.

You can find more information about *Accepted Manuscripts* in the **Information for Authors**.

Please note that technical editing may introduce minor changes to the text and/or graphics, which may alter content. The journal's standard **Terms & Conditions** and the **Ethical guidelines** still apply. In no event shall the Royal Society of Chemistry be held responsible for any errors or omissions in this *Accepted Manuscript* or any consequences arising from the use of any information it contains.

Electrodynamics of soft multilayered particles dispersions:
Dielectric permittivity and dynamic mobility.

Jenny Merlin,[1,2*] Jérôme F.L. Duval[1,2]

[1] Université de Lorraine, Laboratoire Interdisciplinaire des Environnements Continentaux (LIEC), UMR 7360, 15 avenue du Charmois, Vandœuvre-lès-Nancy, F-54501, France.

[2] CNRS, Laboratoire Interdisciplinaire des Environnements Continentaux (LIEC), UMR 7360, 15 avenue du Charmois, Vandœuvre-lès-Nancy, F-54501, France.

*Corresponding author. Email: merlin@sdu.dk

jennymerlin@hotmail.fr

Current address: Institute for Physics, Chemistry and Pharmacy, University of Southern Denmark, Campusvej 55, 5230 Odense, Denmark.

Graphical Abstract.
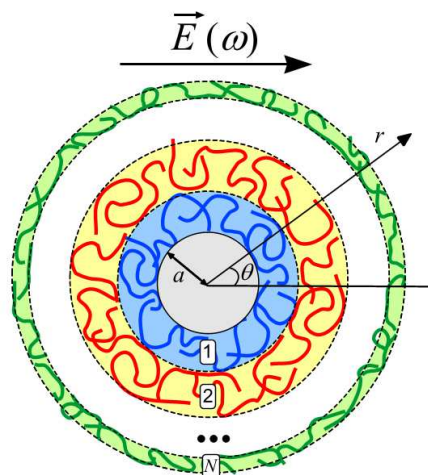
We report a theory for the evaluation of the electrodynamics of dispersions of spherical soft multilayered (bio)particles, with microorganisms and polyelectrolyte multilayers-coated particles as illustrative paradigms. These particles generally consist of a hard (ion- and water-impermeable) core component supporting a succession of step-function or diffuse-like concentric soft (permeable) polymeric layers defined by distinct electrostatic, hydrodynamic and structural properties. The formalism is based on a rigorous numerical resolution of the coupled Navier-Stokes-Brinkman equation, continuity equations for the flow and for the ionic species present in solution, and the non-linear Poisson equation corrected for the multilayered nature of the soft interphase. The frequency-dependent dynamic mobility and dielectric

permittivity of such soft particles suspensions are discussed as a function of the key electrohydrodynamic features of the constituting particulate peripheral layers and solution salinity.

1   **Electrodynamics of soft multilayered particles dispersions:**

2   **Dielectric permittivity and dynamic mobility.**

3   Jenny Merlin,[1,2*] Jérôme F.L. Duval[1,2]

4

5   [1] Université de Lorraine, Laboratoire Interdisciplinaire des Environnements Continentaux (LIEC),

6   UMR 7360, 15 avenue du Charmois, Vandœuvre-lès-Nancy, F-54501, France.

7   [2] CNRS, Laboratoire Interdisciplinaire des Environnements Continentaux (LIEC), UMR 7360, 15

8   avenue du Charmois, Vandœuvre-lès-Nancy, F-54501, France.

9

10   [*]Corresponding author. Email: merlin@sdu.dk

11   jennymerlin@hotmail.fr

12   Current address: Institute for Physics, Chemistry and Pharmacy, University of Southern Denmark,

13   Campusvej 55, 5230 Odense, Denmark.

14

15   **Abstract.**

16   We report a theory for the evaluation of the electrodynamics of dispersions of spherical soft

17   multilayered (bio)particles, with microorganisms and polyelectrolyte multilayers-coated particles as

18   illustrative paradigms. These particles generally consist of a hard (ion- and water-impermeable)

19   core component supporting a succession of step-function or diffuse-like concentric soft (permeable)

20   polymeric layers defined by distinct electrostatic, hydrodynamic and structural properties. The

21   formalism is based on a rigorous numerical resolution of the coupled Navier-Stokes-Brinkman

22   equation, continuity equations for the flow and for the ionic species present in solution, and the non-

23   linear Poisson equation corrected for the multilayered nature of the soft interphase. The frequency-

24   dependent dynamic mobility and dielectric permittivity of such soft particles suspensions are

25   discussed as a function of the key electrohydrodynamic features of the constituting particulate

26   peripheral layers and solution salinity. It is shown that the frequency dependent permittivity is

27   mostly affected by the total charge carried by the overall soft interphase. In contrast, the dynamic

28   mobility is mainly determined by the charge and friction characteristics of the layers located within

29   an electrokinetically-active outer particle region whose extension is defined by the electric double

30   layer thickness and the Brinkman length. Results highlight that under particular electrolyte

31   concentration and layer-to-layer thickness ratio conditions, the dynamic mobility may reflect the

32   physico-chemical and structural properties of the only innermost layers of the soft particle coating.

1. Introduction

Over the past decades, growing attention has been devoted to the understanding of electrokinetic phenomena that involve complex biotic and abiotic colloids like bacteria, viruses, humics and polysaccharides, to quote only a few.[1] These systems may be viewed as paradigms of so-called soft particles because they partly or entirely consist of a charged (polymeric) material that is permeable to ions and hydrodynamic flow.[2] Numerous experimental and theoretical studies have established that the electrokinetic properties of these soft particles dramatically differ from those of their hard (impermeable) counterparts.[2-6] In particular, documented experimental and theoretical studies have demonstrated the inapplicability of the zeta-potential concept to properly explain the electrohydrodynamic features of soft particles.[2-12] Theories are now available to analyse the dependence of their electrophoretic mobility on electric double layer (EDL) thickness, hydrodynamic softness, particle size/charge/concentration and segment density distribution across the soft particle component.[2, 3, 5, 6, 11] These models apply to situations where particle EDLs extending within and outside the charged polymeric material, experience a constant, frequency-independent applied electric field. This allows a complete relaxation of the ionic interfacial processes operating during particles' migration, and the setting of a steady-state situation. The necessity to account for the dynamics of EDL relaxation was recognized long ago from the observation that typical interaction time between charged particles may be too short to allow complete re-equilibration of their overlapping electric double layers upon approach.[13] Accordingly, theoretical models were developed to define the dynamic features of particle EDLs and were further collated with electroacoustic and dielectric experiments. The latter do mimic indeed the complex perturbations of coupled electrohydrodynamic fields and ion-transport fluxes met during particle-particle interactions.[13] Recent work further underlined the importance of treating EDLs at a non-equilibrium level for analysing the dynamics of association/dissociation between target species like metal ions and ligands distributed in charged polymers.[14]

While electrodynamics of EDLs formed in the vicinity of hard (impermeable) particles have been evaluated in much detail,[15-24] few numerical studies only have examined the case of soft permeable particles,[25-30] despite the ubiquitous presence of the latter in *e.g.* natural aquatic media. In particular, Ahualli *et al.*[28] developed a formalism that addresses the frequency-dependent mobility and dielectric permittivity of concentrated suspensions of soft spherical particles composed of a hard core supporting a permeable and homogeneous soft surface layer. This pragmatic

2

1 representation, however, is rarely applicable for real (bio)colloids like bacteria or microgels whose

2 distribution of surrounding polymeric material is typically diffuse (or heterogeneous).[1, 3] It is then

3 necessary to integrate within advanced electrokinetic models a radial dependence for the density of

4 peripheral soft material to be consistent with *e.g.* neutron reflectivity or neutron scattering

5 experiments[1, 31, 32] and to understand *e.g.* swelling properties of soft polymers whether they are

6 supported by particles or macroscopic flat surfaces.[3, 33] Uppapalli and Zhao[30] thus developed an

7 electrodynamic modelling for heterogeneous soft particles, *albeit* within the limit of infinitely

8 diluted suspensions.

9 Despite these important developments, current electrodynamic theories remain inappropriate for

10 soft multilayered interphases defined by a succession of ion-/water-permeable polymeric layers

11 with different chemical composition and distinct electrohydrodynamic features. Though these

12 systems are recurrently found in biology and (bio)material science, they have received so far little

13 attention in the electrokinetic literature. Illustrative representatives include microbial interphases

14 where the soft biomembrane supports one or several types of soft surface appendages (*e.g. pili*,

15 *fimbriae*, polysaccharides),[1, 8, 9] viral particles whose internal RNA or DNA component is

16 encapsulated by a proteic surface layer,[10, 12] polyelectrolyte multilayers,[34] charged polymers

17 supporting synthetic lipidic membranes,[34] or natural rubber particles whose soft interfaces are

18 spatially structured in the form of successive proteins- and phospholipids-rich regions.[35] In

19 agreement with experiments, recent theories by Duval and collaborators[10, 34] demonstrated how the

20 measured dc electrophoretic mobility and streaming current of these particulate and macroscopic

21 soft multilayered systems reflect the electrohydrodynamic properties of their constituting layers to

22 an extent that depends on their respective thickness/charge density, on the flow field penetration

23 (Brinkman) length scale and on the extension of the electric double layer within the interphase. The

24 most striking manifestation of the defining chemical stratification of a soft multilayered interphase

25 is perhaps the marked sigmoid-like dependence of their points of zero electrophoretic mobility and

26 zero streaming current on electrolyte concentration.[34, 35] This fundamental property can be exploited

27 to achieve a refined structural characterization of biointerphases, as recently done for complex

28 natural rubber particles.[35]

29

30 The purpose of this work is to extend our previous dc theory on electrophoresis of soft

31 particulate multilayered particles[10] to the case where they are subjected to an alternating (ac)

32 electric field. The main objective is then to capture how the frequency-dependence of the dynamic

3

1   mobility of soft multilayered particles and that of their dielectric permittivity depend on the charge

2   density, thickness and heterogeneity of the successive constituting soft layers. Analysis is

3   performed over a range of electrolyte concentrations covering the regimes of thin and thick electric

4   double layer as compared to particle size, and for any number of soft layers surrounding the hard

5   core component of the particle. In addition, the theory may be applied to situations where particle

6   concentration requires the account of particle-particle electrohydrodynamic interactions, which is

7   necessary at sufficiently large particle volume fractions. Though this study is mainly concerned

8   with AC electrokinetics of soft multi-layered particles in the dilute regime, analysis of the influence

9   of the volume fraction is briefly reported in Supporting Information (Figure S1). In a first part, the

10 problem is clearly defined and the governing equations required for the evaluation of the dynamic

11 electrophoretic mobility and dielectric permittivity of soft multilayered particles are reported. In a

12 second part, results are discussed along the aforementioned objectives.

13

14 **2. Theory**

15 **2.1. Nomenclature**

16   In the following, the electrokinetic response of a concentrated suspension of soft multilayered

17 spherical particles is evaluated under conditions where an ac electric field $\vec{E}(\omega)$ is applied, where

18 ω is the field pulsation. The radius of the (impermeable) particle hard core is denoted a, and the soft

19 part of the particles consists in a succession of N concentric ion- and water-permeable polymeric

20 layers of thickness d_i. To each soft layer around the particles, we assign the index i, where $i = 1$

21 pertains to the internal layer that is directly supported by the particle core and $i = N$ to the outermost

22 external layer that directly faces the electrolyte solution (Figure 1A). In line with practical systems,

23 the formalism further integrates the possibility of a gradual transition for the distribution of polymer

24 segment density between two adjacent layers (Figure 1B). Assuming homogeneous distribution of

25 fixed (immobile) charged sites along a given polymer segment, the volume charge density

26 throughout the diffuse multilayered interphase, $\rho_{\text{fix}}(r)$, may be written in the form:[10, 36]

27 $$\rho_{\text{fix}}(r) = \rho_N^0 g(r),\tag{1}$$

28 with $$g(r) = \chi\left[\sum_{i=1}^{N-1}(\beta_i - \beta_{i+1})f_i(r) + f_N(r)\right]\tag{2}$$

1   and
$$f_i(r) = \frac{1}{2}\left(1 - \tanh\left[\frac{r - \sum_{j=1}^{i} d_j}{\alpha_i}\right]\right),$$ (3)

2   where α_i denotes the typical length over which the polymer segment density within layer i deviates

3   from a step function-like profile. The limit $\alpha_i \to 0$ reduces to a homogeneous distribution of

4   polymer segments within layer i (marked by a dashed curve in Figure 1B) where the density of

5   fixed (immobile) is then denoted as ρ_1^0. Cases $\alpha_i\,(>0)$ pertain to a diffuse distribution of polymer

6   segments (plain curve in Figure 1B). This representation of gradual distribution of polymer segment

7   density across the soft interphase has been originally introduced by Hill et al.[5] Later Duval and

8   Ohshima[3] detailed the impact of diffuse segment density distribution on DC soft surface

9   electrokinetics. The choice of the tanh-like function in equation (3) is motivated by the fact that this

10   function is regularly employed to fit SANS and neutron reflectivity data collected on soft polymeric

11   systems.[37, 38] It is also recurrently found in mean field polymer physics to evaluate volume density

12   distribution across polymer layers.[39]   In eqn (2), the dimensionless scalar β_i is defined by

13   $\beta_i = \rho_1^0 / \rho_N^0$ and ρ_N^0 may be expressed in the form $\rho_N^0 = z_N F c_N^*$ where z_N and c_N^* are the valence

14   and molar concentration of charge sites within layer N and F is the Faraday. Equations (1) and (2)

15   remain valid for other choice of the function $f_i(r)$ than that formulated by eqn (3) providing that

16   the limit of $g(r)$ for $r \to \infty$ remains zero. The scalar χ in eqn (2) ensures that a constant total

17   number of charges within the whole soft multilayered interphase is maintained upon variation of the

18   quantity α_i.[3] It therefore satisfies the relationship:[10]

19
$$\chi = \sum_{k=1}^{N} \beta_i \left\{\left(a + \sum_{i=1}^{k} d_i\right)^3 - \left(a + \sum_{i=1}^{k-1} d_i\right)^3\right\} \bigg/ \left\{3\int_0^\infty r^2 g(r)\,dr\right\}$$ (4)

20   The polymer segments across the soft interphase are further regarded as resistance centres exerting

21   frictional forces on the electroosmotic flow that develops within/around the particle. For sufficiently

22   dilute polymer phases, the local friction coefficient $k(r)$ may then be directly related to the

23   polymer segments density distribution throughout the interphase according to

24
$$k(r) = k_N^0 g^H(r),$$ (5)

5

1 with k_N^0 the friction coefficient in the external layer N for $\alpha_N \to 0$. The function $g^{\mathrm{H}}(r)$ in eqn (5)

2 is the hydrodynamic counterpart of $g(r)$. It is formulated according to

$$g^{\mathrm{H}}(r) = \chi^{\mathrm{H}}\left[\sum_{i=1}^{N-1}\left(\beta_i^{\mathrm{H}} - \beta_{i+1}^{\mathrm{H}}\right)f_i(r) + f_N(r)\right] \tag{6}$$

4 with, $$\chi^{\mathrm{H}} = \sum_{k=1}^{N}\beta_i^{\mathrm{H}}\left\{\left(a + \sum_{i=1}^{k}d_i\right)^3 - \left(a + \sum_{i=1}^{k-1}d_i\right)^3\right\}\bigg/\left\{3\int_0^{\infty}r^2 g^{\mathrm{H}}(r)\,\mathrm{d}r\right\}, \tag{7}$$

5 where χ^{H} is a constant defined in such a way that the total amount of polymer segments within the

6 soft permeable part of the particle is constant with changing interphasial diffuseness.[10] The scalar

7 parameters $\beta_i^{\mathrm{H}}\,(>0)$ are given by $\beta_i^{\mathrm{H}} = k_i^0/k_N^0$ where k_i^0 is the friction coefficient within layer i for

8 $\alpha_i \to 0$. The spatial distribution of the so-called hydrodynamic softness, $\lambda(r)$, is then provided by:

$$\lambda(r) = \left(k(r)/\eta\right)^{1/2} \tag{8}$$

10 where η is the viscosity of the medium. The quantity $\lambda^{-1}(r)$ has the dimension of a length and

11 represents the local penetration of electroosmotic flows within the particle. Combining eqns (5) and

12 (8) gives:

$$\lambda(r) = \lambda_N^0\left[g^{\mathrm{H}}(r)\right]^{1/2}, \tag{9}$$

14 where $1/\lambda_N^0$ denotes the hydrodynamic penetration length within layer N for $\alpha_N \to 0$.

15 The particles described above are dispersed into an electrolyte solution containing M ionic

16 species with bulk concentrations c_k^*, valences z_k and drag coefficients λ_k $(k = 1\ldots M)$. The medium

17 is defined by its viscosity η and its static dielectric permittivity $\varepsilon_0\varepsilon_{\mathrm{r}}$ with ε_{o} the vacuum

18 permittivity and ε_{r} the relative permittivity of the medium. We assume here that both η and $\varepsilon_0\varepsilon_{\mathrm{r}}$

19 within the soft particle component are constant and equal to their corresponding bulk values, which

20 is correct for sufficiently dilute polymer phases.[1] The drag coefficient of ion k is related to the

21 corresponding limiting conductance Λ_k^{o}:

22 $k = 1\ldots M,$ $$\lambda_k = \frac{N_{\mathrm{A}}e^2|z_k|}{\Lambda_k^{\mathrm{o}}}. \tag{10}$$

23 The formalism further allows the account of the finite volume fraction ϕ of particles in the

24 dispersion. For that purpose, the so-called cell-model, originally introduced by Kuwabara,[40] is

25 adopted. In details, the spherical soft multilayered particle, with hard core radius a is enclosed in a

1   concentric cell, with radius $b > a + \sum_{i=1}^{N} d_i$, so that the volume fraction of solids ϕ in the cell model is

2   identical to that in the overall solution (Figure 1C), leading to $\phi = a^3/b^3$. This definition of ϕ is

3   based on the hard core radius of the particle and not the overall radius of the particle with both hard

4   and soft particle components included. It thus circumvents the difficulty to define for a diffuse

5   interphasial segment density profile, the frontier between the N-th layer and the outer electrolyte

6   solution, though pragmatic solutions to do so are given in the literature.[3]

7

8   **2.2. Governing electrodynamic equations for soft multilayered particles**

9   **2.2.1. Equilibrium electrostatic potential distribution**

10   The analysis of the electrodynamics of soft multilayered particle dispersion first requires a

11   description of the equilibrium situation, *i.e.* in the absence of the externally applied ac field. At

12   equilibrium, the concentration of free ions $c_k^e(r)$ in the medium and within the soft particle envelop

13   follows Boltzmann statistics

14   $k = 1...M,$ $$c_k^e(r) = c_k^* \exp\left(-\frac{z_k F}{RT}\Psi^e(r)\right) = c_k^* \exp\left(-z_k y^e(r)\right),$$ (11)

15   where R is the gas constant, T the temperature, $\Psi^e(r)$ the local equilibrium electrostatic potential

16   and $y^e(r) = F\Psi^e(r)/RT$ the corresponding dimensionless potential. $\Psi^e(r)$ is governed by the

17   Poisson equation written

18   $$\nabla^2 \Psi^e(r) = -\frac{\rho_{el}^e(r)}{\varepsilon_0 \varepsilon_r} - \frac{\rho_{fix}(r)}{\varepsilon_0 \varepsilon_r} = -\frac{1}{\varepsilon_0 \varepsilon_r}\sum_{k=1}^{M} z_k F c_k^e(r) - \frac{\rho_{fix}(r)}{\varepsilon_0 \varepsilon_r},$$ (12)

19   with $\rho_{el}^e(r)$ the volume charge density stemming from the distribution of the free ions at

20   equilibrium. ∇^2 is the Laplacian operator given by $\nabla^2 \bullet = \frac{1}{r^2}\frac{d}{dr}\left[r^2\frac{d\bullet}{dr}\right]$. Combining eqns (11) and

21   (12) provides the Poisson-Boltzmann equation that governs the equilibrium electrostatic potential

22   distribution within the cell model:

23   $$\tilde{\nabla}^2 y^e(x) = -\frac{1}{\sum_{k=1}^{M} z_k^2 c_k^*}\left[\sum_{k=1}^{M} z_k c_k^* \exp\left(-z_k y^e(x)\right) + z_N c_N^* g(x)\right]$$ (13)

1   where we have introduced the scaled radial position $x = \kappa(r-a)$ and the dimensionless Laplacian

2   operator $\tilde{\nabla}^2 \bullet = \kappa^{-2}\nabla^2 \bullet = \dfrac{1}{(x+\kappa a)^2}\dfrac{d}{dx}\left[(x+\kappa a)^2\dfrac{d\bullet}{dx}\right]$. κ is the reciprocal Debye length defined by

3    $\kappa = \left[\sum_{k=1}^{M} F^2 z_k^2 c_k^* \big/ RT\varepsilon_0\varepsilon_r\right]^{1/2}$. The first boundary condition associated to eqn (13) reflects that the

4   hard core of the particles carries a surface charge density σ_s:[3]

5
$$\left.\frac{dy^e(x)}{dx}\right|_{x=0} = -\frac{F\sigma_s}{\kappa\varepsilon_0\varepsilon_r RT}. \tag{14}$$

6   Electroneutrality in the Kuwabara unit cell leads to the following boundary condition at $r = b$:

7
$$\left.\frac{dy^e(x)}{dx}\right|_{x=\kappa(b-a)} = 0. \tag{15}$$

8   We emphasize that there is no need for introducing additional boundary conditions because of the

9   use of the continuous functions $g(r)$ and $g^H(r)$ in the modelling of the soft multilayered

10   interphase. The set of eqns (13), (14) and (15) therefore rigorously defines the spatial equilibrium

11   distribution of the potential and the relevant ion concentrations across the cell.

12

13   **2.2.2. Frequency-dependent perturbations of the local ion concentrations and**

14   **electrostatic potential distribution**

15   In line with electrodynamic experiments, the magnitude of the applied electric field is small

16   enough to keep the response of the system linear with respect to the field. The resulting time-

17   dependent potential and concentration profiles, denoted as $\Psi(\vec{r},t)$ and $c_k(\vec{r},t)$, respectively, may

18   then be written as the sum of their equilibrium value and a first-order field-induced perturbation

19   term according to:

20
$$X(\vec{r},t) = X^e(r) + \delta X(\vec{r})e^{j\omega t}, \tag{16}$$

21   where j is the imaginary number $j^2 = 1$ and t is the time. X represents any of the frequency-

22   dependent variables of the problem. The field-induced perturbation terms being small as compared

23   to the corresponding equilibrium value, it is then legitimate to disregard products of field-induced

24   perturbation terms.

25   Our objective is to determine the dynamic velocity of the particle and the dielectric permittivity

26   of the particle dispersions as a function of ω, which requires the evaluation of the perturbation terms

1     $\delta\Psi(\vec{r})$ and $\delta c_k(\vec{r})$. For that purpose, the formalism is based on the standard set of electrokinetic

2   equations corrected for the diffuse multilayered nature of the soft interphases examined in this

3   work. In particular, the velocity of the fluid with respect to the particle is determined from solution

4   of the Navier-Stokes-Brinkman equation, the concentration profiles of the electrolyte ions within

5   the multi-layered interphase are solved using the relevant continuity equations for each ionic

6   species and the potential profile across the multilayered interphase is determined from non-linear

7   Poisson equation. The resulting set of differential equations is then solved for a given ω. The

8   formalism ignores the possible deformation of the soft layers under action of the applied electric

9   field, an approximation that is justified providing that the stiffness of the layers is sufficiently large

10   to counteract the electrostatic/osmotic stresses within the soft layers.

11   The Navier-Stokes equation then reads:

12 $$\eta\nabla\times\nabla\times\vec{u}(\vec{r},t)+\nabla P(\vec{r},t)+\rho_{el}(\vec{r},t)\cdot\nabla\Psi(\vec{r},t)+k(r)\vec{u}(\vec{r},t)=\rho_m\frac{\partial\vec{u}(\vec{r},t)}{\partial t}, \tag{17}$$

13   where $\vec{u}(\vec{r},t)=\vec{u}(\vec{r})e^{j\omega t}$ is the flow velocity counted with respect to the particle, $P(\vec{r},t)$ is the

14   pressure, $\rho_{el}(\vec{r},t)$ is the charge density resulting from distribution of the ionic species and ρ_m is the

15   mass density of the medium. In eqn (17), the Reynolds numbers of the liquid flowing within and

16   outside the soft layers are sufficiently small to ignore inertial terms, and the fluid is further

17   considered in the incompressible limit. We introduce the field-induced perturbation term $\delta\mu_k(\vec{r})$ of

18   the electrochemical potential of ion k:

19    $k=1\ldots M,$ $\mu_k(\vec{r},t)=\mu_k^e+\delta\mu_k(\vec{r})e^{j\omega t}=\mu_k^\infty+z_kF\Psi(\vec{r},t)+RT\ln c_k(\vec{r},t)$ (18)

20   where μ_k^∞ is the standard chemical potential of ion k. Using eqns (16) and (18), $\delta\mu_k(\vec{r})$ can be

21   rewritten in the form

22    $k=1\ldots M,$ $$\delta\mu_k(\vec{r})=z_kF\delta\Psi(\vec{r})+RT\frac{\delta c_k(\vec{r})}{c_k^e(r)}. \tag{19}$$

23   On the basis of spherical symmetry considerations, $\vec{u}(\vec{r})$ can be further expressed according to:[2]

24 $$\vec{u}(\vec{r})=\left(-\frac{2}{r}h(r)E\cos\theta,\frac{1}{r}\frac{d}{dr}(rh(r))E\sin\theta,0\right) \tag{20}$$

25   where $h(r)$ is a function of r only. $\delta\Psi(\vec{r})$ et $\delta\mu_k(\vec{r})$ can be defined as:[2]

26 $$\delta\Psi(\vec{r})=\delta\psi(r)\vec{E}\cdot\vec{r}/\|\vec{r}\|=\delta\psi(r)E\cos\theta$$
$$\delta\mu_k(\vec{r})=-z_kF\varphi_k(r)\vec{E}\cdot\vec{r}/\|\vec{r}\|=-z_kF\varphi_k(r)E\cos\theta. \tag{21 a,b}$$

9

1   Following Ohshima's methodology[1] and combining eqn (17) with eqns (18)-(21a,b), we obtain after

2   algebraic developments,

$$L\left(\left[L+\gamma^{2}\right]h(r)\right)-G(r)=-\frac{F}{\eta r}\frac{dy^{e}(r)}{dr}\sum_{k=1}^{M}\left[z_{k}^{2}c_{k}^{*}e^{-z_{k}y^{e}(r)}\varphi_{k}(r)\right], \tag{22}$$

4   where L is the differential operator $L\bullet = d^{2}\bullet/dr^{2}+(2/r)d\bullet/dr-2\bullet/r^{2}$, γ^{2} the quantity

5    $\gamma^{2}=j\omega\rho_{m}/\eta$ and $G(r)$ the function defined by:

$$G(r)=\left(\lambda_{N}^{0}\right)^{2}\left\{g^{H}(r)Lh(r)+\frac{dg^{H}(r)}{dr}\left(\frac{dh(r)}{dr}+\frac{h(r)}{r}\right)\right\}. \tag{23}$$

7   In the limit where particles hard core is enveloped by a single soft layer of thickness d_{1} with

8   homogeneous polymer segments distribution, eqn (22) satisfactorily reduces to the differential

9   equation derived by Ahualli et al.[28] where $G(r) = 0$ in the medium ($d_{1} < r < b$) and $G(r) =$

10   $(\lambda_{1}^{0})^{2}Lh(r)$ in the soft layer ($a < r < d_{1}$). In addition, under static conditions, i.e. in the presence of

11   a dc applied electric field, the frequency-dependent parameter γ^{2} vanishes and eqn (22) then

12   correctly simplifies into the result derived by Duval and Ohshima in their dc electrophoresis of

13   spherical soft multilayered particles.[3]

14   The continuity equation for each ion k ensures a constant total number of ions in the cell so

15   that:

16   $k = 1…M,$
$$\frac{\partial c_{k}(\vec{r},t)}{\partial t}=-\nabla\left(c_{k}(\vec{r},t)\vec{v}_{k}(\vec{r},t)\right) \tag{24}$$

17   where $\vec{v}_{k}(\vec{r},t)$ is the local velocity of ion k with convective, conductive and diffusive contributions:

18   $k = 1…M,$
$$\vec{v}_{k}(\vec{r},t)=\vec{u}(\vec{r},t)-\frac{1}{N_{A}\lambda_{k}}\nabla\mu_{k}(\vec{r},t). \tag{25}$$

19   In the incompressible fluid, $\nabla\cdot\vec{u}(\vec{r},t)=0$ and combination with eqns (16), (18), (24) and (25) leads

20   to :

21   $k = 1…M,$
$$j\omega\delta c_{k}(\vec{r})=-\nabla\left\{c_{k}^{e}(r)\vec{u}(\vec{r})-\frac{1}{N_{A}\lambda_{k}}c_{k}^{e}(r)\nabla\delta\mu_{k}(\vec{r})\right\}. \tag{26}$$

22   Substitution of eqns (20) and (21a,b) into eqn (26) then gives the following expression for each ion

23   k:

24   $k = 1…M,$
$$L\varphi_{k}(r)+\kappa^{2}\gamma_{k}^{2}\left(\varphi_{k}(r)+\delta\psi(r)\right)=\frac{dy^{e}(r)}{dr}\left[z_{k}\frac{d\varphi_{k}(r)}{dr}-2\frac{\lambda_{k}}{e}\frac{h(r)}{r}\right] \tag{27}$$

1   with $\gamma_k^2 = j\omega\lambda_k N_A / (\kappa^2 RT)$ $(k = 1...M)$ and $\varphi_k(r)$ is defined in eqn (21b).

2   The Poisson equation applied to the field-induced perturbation terms reads:

3
$$\nabla^2 \delta\Psi(\vec{r}) = -\frac{1}{\varepsilon_0 \varepsilon_r} \sum_{k=1}^{M} z_k F \delta c_k(\vec{r}).$$
(28)

4   Using eqns (19) and (21b), we finally obtain for $\delta\psi(r)$ defined in eqn (21a):

5
$$L\delta\psi(r) = \frac{1}{\varepsilon_0 \varepsilon_r} \sum_{k=1}^{M} \left\{ \frac{z_k^2 F^2}{RT} c_k^e(r) \left[\varphi_k(r) + \delta\psi(r) \right] \right\}.$$
(29)

6

7   **2.3. Setting the boundary conditions for the field-induced perturbation terms**

8   The setting of the appropriate set of boundary conditions associated with the differential

9   equations (22), (27) and (29) has already been detailed in previous studies.[23, 24, 41] We briefly report

10   below the main results.

11   **2.3.1. Conditions satisfied at the hard core surface of the particle ($r = a$)**

12   The slipping plane where $\vec{u}(\vec{r}) = 0$ is located at the hard (flow-impermeable) core surface.

13   Using eqn (20), it comes:

14
$$h(a) = 0$$
(30)

15   and
$$\left. \frac{dh(r)}{dt} \right|_{r=a} = 0.$$
(31)

16   By definition, the hard core is impermeable to electrolyte ion k, which implies $\vec{v}_k(\vec{r},t) \cdot \vec{e}_n = 0$

17   where $\vec{e}_n$ is the normalized vector normal to the particle core surface. In turn, we have

18   $k = 1...M,$
$$\left. \frac{d\varphi_k(r)}{dr} \right|_{r=a} = 0.$$
(32)

19   Finally, the continuity of the potential and the normal component of the electric field displacement

20   provides:

21
$$\left. \frac{d\delta\psi(r)}{dr} \right|_{r=a} - \frac{\varepsilon_p}{\varepsilon_r a} \delta\psi(a) = 0$$
(33)

22   where ε_p is the relative dielectric permittivity of the hard particle core.

23   **2.3.2. Conditions satisfied at the Kuwabara unit cell surface ($r = b$)**

11

1   In order to determine the relevant boundary conditions at $r = b$, we consider the average values

2   of $f(\vec{r})$ (with $f(\vec{r})$ a dummy function that identifies to $\delta c_k(\vec{r})$ or $P(\vec{r})$) within a cell volume V:[41]

$$\langle f(\vec{r}) \rangle = \frac{1}{V} \int_V f(\vec{r}) \, dV \, . \tag{34}$$

4   The definition of the electric field $\langle -\nabla \delta \Psi(\vec{r}) \rangle = \langle E \rangle$ implies:[23, 41]

$$\delta \psi(b) = -b \, . \tag{35}$$

6   Let's consider that the particle displacement only results from electrophoresis (no diffusiophoresis

7   contribution). Then, the condition $\langle \nabla \delta c_k(\vec{r}) \rangle = 0$ gives:[23, 41]

$$\varphi_k(b) = b \, . \tag{36}$$

9   The particle displacement does not result from convective contribution, leading to $\langle \nabla P(\vec{r}) \rangle = 0$ so

10   that $P(b) = 0$ and[23, 41]

$$\frac{d}{dr} \left[r \left(L + \gamma^2 \right) h(r) \right] \bigg|_{r=b} = \frac{\rho_{el}^e(b)}{\eta} b + \mu_e \gamma^2 b, \tag{37}$$

12   with μ_e the dynamic mobility that is proportional to the liquid velocity relative to the particle (μ_e

13   does not depend on the magnitude of the applied field). Based on experiment results using ESA

14   (Electrokinetic Sonic Amplitude), O'Brien *et al.* showed that the theoretical dynamic mobility can

15   correctly predict experimental results only if the average momentum per unit mass is zero.[42, 43] The

16   relation $(1/\rho V) \int_V \rho(\vec{r}) \vec{u}(\vec{r}) dV = 0$ then must be satisfied (with $\rho = \rho_p$ in the hard core and

17   $\rho = \rho_m$ in the soft interphase and the bulk solution), which provides

$$\mu_e = \frac{2h(b)}{b} \left(1 + \phi \frac{\rho_p - \rho_m}{\rho_m} \right)^{-1} . \tag{38}$$

19   The last boundary condition stems from the zero vorticity condition at the Kuwabara cell surface

20   $\left(\nabla \times \vec{u}(\vec{r}) \right)\big|_{r=b} = 0$.[20, 22] Using the latter condition, eqn (20) then becomes:

$$Lh(r)\big|_{r=b} = 0 \, . \tag{39}$$

22   For the sake of simplicity and mathematical convenience, we use for the numerical

23   computation of the governing electrodynamic equations the following scaled quantities:

$$\delta\tilde{\psi}(r) = \kappa \delta\psi(r) \; ; \; \tilde{\varphi}_k(r) = \kappa \varphi_k(r) \; ; \; \tilde{h}(r) = \frac{\kappa F \eta}{\varepsilon_0 \varepsilon_r RT} h(r) \; ; \; \tilde{\lambda}_N^0 = \kappa^{-1} \lambda_N^0$$

1

$$\tilde{\gamma}^2 = \kappa^{-2}\gamma^2 \;\; ; \;\; \tilde{L}\bullet = \kappa^{-2}L\bullet = \frac{\mathrm{d}^2 \bullet}{\mathrm{d}x^2} + \frac{2}{x+\kappa a}\frac{\mathrm{d}\bullet}{\mathrm{d}x} - \frac{2}{(x+\kappa a)^2}\bullet \tag{40}$$

2   Using eqn (40), we show after some developments that the set of differential equations (22), (27)

3   and (29) may be written in the form:

4

$$\begin{cases}
\tilde{L}\left(\left[\tilde{L}+\tilde{\gamma}^2\right]\tilde{h}(x)\right)-\left(\tilde{\lambda}_N^0\right)^2\left\{g^H(x)\tilde{L}\tilde{h}(x)+\frac{\mathrm{d}g^H(x)}{\mathrm{d}x}\left(\frac{\mathrm{d}\tilde{h}(x)}{\mathrm{d}x}+\frac{\tilde{h}(x)}{x+\kappa a}\right)\right\} \\
\qquad = -\frac{1}{\displaystyle\sum_{k=1}^{M} z_k^2 c_k^*}\frac{1}{x+\kappa a}\frac{\mathrm{d}y^e(x)}{\mathrm{d}x}\sum_{k=1}^{M}\left\{z_k^2 c_k^* e^{-z_k y^e(x)}\tilde{\varphi}_k(x)\right\}, \\[2mm]
L\tilde{\varphi}_k(x)+\gamma_k^2\left(\tilde{\varphi}_k(x)+\delta\tilde{\psi}(x)\right)=\frac{\mathrm{d}y^e(r)}{\mathrm{d}r}\left[z_k\frac{\mathrm{d}\tilde{\varphi}_k(x)}{\mathrm{d}r}-2\frac{\lambda_k}{e}\frac{\varepsilon_0\varepsilon_r RT}{F\eta}\frac{\tilde{h}(x)}{x+\kappa a}\right], \\[2mm]
\tilde{L}\delta\tilde{\psi}(x)=\frac{1}{\displaystyle\sum_{k=1}^{M} z_k^2 c_k^*}\sum_{k=1}^{M}\left\{z_k^2 c_k^* e^{-z_k y^e(x)}\left[\tilde{\varphi}_k(x)+\delta\tilde{\psi}(x)\right]\right\},
\end{cases} \tag{41}$$

5   Similarly, the associated boundary conditions on the core surface (eqns (30)-(33)) become:

6

$$\begin{cases}
\left.\dfrac{\mathrm{d}\delta\tilde{\psi}(x)}{\mathrm{d}x}\right|_{x=0} - \dfrac{\varepsilon_p}{\kappa a\varepsilon_r}\delta\tilde{\psi}(0)=0, \\[2mm]
\left.\dfrac{\mathrm{d}\delta\tilde{\varphi}_k(x)}{\mathrm{d}x}\right|_{x=0} = 0, \\[2mm]
\tilde{h}(0)=0, \\[2mm]
\left.\dfrac{\mathrm{d}\tilde{h}(x)}{\mathrm{d}x}\right|_{x=0} = 0,
\end{cases} \tag{42}$$

7   and the conditions on the Kuwabara cell surface (eqns (35)-(37) and (39)) lead to:

8

$$\begin{cases}
\delta\tilde{\psi}(\kappa(b-a))=-\kappa b, \\[2mm]
\tilde{\varphi}_k(\kappa(b-a))=\kappa b, \\[2mm]
\left.\tilde{L}\tilde{h}(x)\right|_{x=\kappa(b-a)}=0, \\[2mm]
\left.\dfrac{\mathrm{d}}{\mathrm{d}x}\left[\left(\tilde{L}+\tilde{\gamma}^2\right)\tilde{h}(x)\right]\right|_{x=\kappa(b-a)}=\dfrac{\displaystyle\sum_{k=1}^{M} z_k^2 c_k^* e^{-z_k y^e(\kappa(b-a))}}{\displaystyle\sum_{k=1}^{M} z_k^2 c_k^*}+\tilde{\gamma}^2\dfrac{2\tilde{h}(\kappa(b-a))}{\kappa b}\left(-1+\left(2\phi\dfrac{\rho_p-\rho_m}{\rho_m}\right)^{-1}\right).
\end{cases} \tag{43}$$

13

1   Equations (41) - (43) fully determine the searched electrohydrodynamic functions $\delta\tilde{\psi}$, $\tilde{\varphi}_k$, $\tilde{h}(r)$

2   (or equivalently $\delta\psi$, φ_k, $h(r)$). We recall below how these functions allow the evaluation of the

3   measurable dynamic mobility of the particles and dielectric permittivity of the particle dispersion.

4

5   **2.4. Evaluation of particle dynamic mobility and particle dispersion dielectric**

6   **permittivity**

7   Both the particle dynamic mobility $\mu_e(\omega)$ and the particle dispersion dielectric permittivity

8    $\varepsilon^*(\omega)$ are complex quantities that may be written in the form:

9    $$\mu_e(\omega) = \mu_e'(\omega) + j\mu_e''(\omega),$$

10   and $$\varepsilon^*(\omega) = \varepsilon'(\omega) - j\varepsilon''(\omega) = \Delta\varepsilon'(\omega) - j\varepsilon''(\omega) + \varepsilon_r, \tag{44}$$

11   where real and imaginary parts are marked by $'$ and $''$, respectively. The dielectric increment

12    $\Delta\varepsilon'(\omega)$ is defined by $\Delta\varepsilon'(\omega) = \varepsilon'(\omega) - \varepsilon_r$. Using eqns (38) and (40), $\mu_e(\omega)$ may be written in the

13   form:

14    $$\mu_e(\omega) = \frac{2\tilde{h}(\kappa(b-a))}{\kappa b} \frac{\varepsilon_0\varepsilon_r RT}{F\eta} \left(1 + \phi\frac{\rho_p - \rho_m}{\rho_m}\right)^{-1}. \tag{45}$$

15    $\mu_e(\omega \to 0)$ corresponds to the dc electrophoretic mobility limit. The dynamic conductivity $K^*(\omega)$

16   is further defined as the sum of the contribution $K_m^*(\omega)$ from the ions in the background electrolyte

17   (in the absence of particles) and that $\Delta K^*(\omega)$ due to the presence of the charged particles:

18    $$K^*(\omega) = K_m^*(\omega) + \Delta K^*(\omega). \tag{46}$$

19    $K_m^*(\omega)$ is simply given by:

20    $$K_m^*(\omega) = \sum_{k=1}^{M} \frac{z_k^2 eFc_k^*}{\lambda_k} - j\omega\varepsilon_0\varepsilon_r. \tag{47}$$

21    $K^*(\omega)$ can be equivalently obtained from the average current $\langle i \rangle$ and electric field $\langle E \rangle$ using

22    $\langle i \rangle = K^*(\omega)\langle E \rangle$. Following the methodology by Bradshaw-Hajek *et al.*[23] and using eqns (46) and

23   (47), $K^*(\omega)$ then becomes:

24    $$\Delta K^*(\omega) = \sum_{k=1}^{M} \frac{z_k^2 eFc_k^*}{\lambda_k} \left[e^{-z_k y^e(\kappa(b-a))} \left.\frac{d\tilde{\varphi}_k(x)}{dx}\right|_{x=\kappa(b-a)} - 1 \right]$$

14

1

$$-\mu_e(\omega)\phi\frac{\rho_p-\rho_m}{\rho_m}\sum_{k=1}^{M}z_k F c_k^* e^{-z_k y^e(\kappa(b-a))} + j\omega\varepsilon_0\varepsilon_r\left[\left.\frac{\mathrm{d}\delta\tilde{\psi}(x)}{\mathrm{d}x}\right|_{x=\kappa(b-a)}+1\right]. \tag{48}$$

2 $K_m^*(\omega)$, $\Delta K^*(\omega)$ and $K^*(\omega)$ are all complex quantities. The latter is connected to $\varepsilon^*(\omega)$ *via*:

3

$$K^*(\omega)=K'(\omega)+jK''(\omega)=K'(\omega\to 0)+\omega\varepsilon_0\varepsilon''(\omega)-j\omega\varepsilon_0\left(\Delta\varepsilon'(\omega)+\varepsilon_r\right) \tag{49}$$

4 Finally, from eqns (46), (47) and (49), $\Delta\varepsilon'(\omega)$ et $\varepsilon''(\omega)$ may be formulated according to :

5

$$\Delta\varepsilon'(\omega)=-\frac{\Delta K''(\omega)}{\omega\varepsilon_0}, \tag{50}$$

6 and

$$\varepsilon''(\omega)=\frac{\Delta K'(\omega)-\Delta K'(\omega\to 0)}{\omega\varepsilon_0}. \tag{51}$$

7

8 ### 2.5. Numerical resolution

9   The complexity of the set of non-linear differential equations (41) with boundary conditions

10 (42) and (43) requires a numerical analysis in order to obtain the equilibrium potential $y^e(x)$ and

11 the searched functions $\delta\tilde{\psi}(x)$, $\tilde{\varphi}_k(x)$ and $\tilde{h}(x)$ as a function of ω. To do so, we developed a

12 FORTRAN code for solving the above set of differential equations over a wide range of field

13 pulsations of practical interest (Hz to MHz) with use of the COLSYS collocation procedure.[44]

14 Following such a strategy, the searched solutions are assimilated to polynomial functions estimated

15 on an auto-adaptive spatial grid with a prescribed accuracy set here to 10^{-4}. The dynamic mobility

16 $\mu_e(\omega)$, dielectric increment $\Delta\varepsilon'(\omega)$ and dielectric loss $\varepsilon''(\omega)$ were then evaluated *via* eqns (45),

17 (48), (50) and (51). The formalism is valid without any restrictions on particle size (hard core radius

18 and soft layers thickness), particle charge, hydrodynamic permeability and number of soft layers.

19 The numerical results were successfully tested with those obtained from the literature. On one hand,

20 the frequency dependence of the mobility and the dielectric permittivity agrees with different

21 analyses of ac electrokinetics of suspensions of hard particles[24] and of soft particles carrying a

22 unique and homogeneous polymeric layer[28] (results presented in Supporting Information, Figure

23 S2). In addition, we successfully verified that in the zero frequency limit, the mobility values

24 obtained from the current formalism correctly reproduce the results by Langlet et *al.*[10] and Rochette

25 et *al.*[35] for the dc electrophoretic mobility of soft multilayered viral and natural rubber particles with

26 diffuse polymer segment density distributions.

27

1   **3.   Results and discussions**

2   In the following sections, we discuss the marked features of the frequency-dependent dielectric

3   permittivity and dynamic mobility of soft multilayered particles. Unless otherwise specified, for the

4   sake of demonstration, we consider particles that consist of a hard core covered by two

5   homogeneous soft surface layers ($\alpha_{i=1,2} \to 0$), suspended in a 1:1 symmetrical electrolyte of

6   concentration c^*. Results are provided for a dilute particle dispersion with $\phi = 0.01$ and the relevant

7   constants used in the illustrative simulations below are further collected in Table 1.

8

9   **3.1. Impact of the charge of the innermost soft surface layer, of the particle**

10   **hydrodynamic softness and of the electrolyte concentration**

11   **3.1.1. Dielectric permittivity**

12   The dependence of the dielectric increment $\Delta\varepsilon'(\omega)$ on frequency $\omega/2\pi$ is displayed in Figures

13   2A-2C for various values of the bulk electrolyte concentration c^*, for different layer charge density

14   ratios $\beta_1 = \rho_1^0 / \rho_2^0$, and for several values of the hydrodynamic softness λ_2^0 normalized with use of

15   the outer soft surface layer thickness, *i.e.* $\lambda_2^0 d_2$. All other parameters are fixed and are reported in

16   the caption of Figures 2A-2C. The insets represent the corresponding variations of the dielectric

17   loss $\varepsilon''(\omega)$. For all situations tested, the dielectric spectra display an expected continuous decrease

18   of $\Delta\varepsilon'(\omega)$ from a low-frequency plateau value to a zero value reached at $\omega \to \infty$. This decrease

19   reflects the classical α-relaxation process reported for ionic particulate EDLs,[45] and it is marked by

20   a maximum in $\varepsilon''(\omega)$ at the characteristic frequency $\omega = \omega_\alpha = 2D_{\text{eff}} / a^2$,[46] where D_{eff} is the effective

21   diffusion coefficient $D_{\text{eff}} = 2D_+D_- / (D_+ + D_-)$ with D_+ and D_- the diffusion coefficients of cations and

22   anions, respectively. The α-relaxation, or concentration polarization, is a low frequency process

23   (typically below 100 kHz) and results from the establishment of a neutral electrolyte gradient

24   around each particle.[45, 46] It is created by diffusive and conductive fluxes of ions within the EDL

25   and the bulk solution following the application of the electric field.[45, 46] As pointed out by Ahualli

26   *et al.*,[28] ω_α is mainly governed by the size of the hard core and not by that of the whole particle, *i.e.*

27   hard core radius plus overall thickness of the soft particle component. The authors showed that the

28   distance at which the neutral electrolyte gradient is formed is basically equivalent for hard and soft

29   particles with same core size a. Let us now detail the results in Figure 2A. The quantities c^* and

30   $\lambda_2^0 d_2$ are fixed and the outermost layer carries a negative charge density $\rho_2^0 / F = -10$ mM.

1 Decreasing the quantity $\beta_1 > 0$ comes to decrease the total amount of fixed (immobile) charges

2 $Q_{tot} = \sum_{i=1,2} V_i \beta_i \rho_2^0$ within the soft bilayered shell of the particle (V_i is the volume of layer i).

3 Accordingly, at fixed frequency, the local electrostatic potential within the EDL decreases in

4 magnitude and so does the amount of counterions (cations) within the soft interphase. As a result,

5 the concentration polarization around the particle becomes less important, which results in a

6 decrease of $\Delta\varepsilon'(\omega)$ with decreasing $\beta_1 > 0$ until a minimum is reached at $\beta_1 = 0$. The latter

7 situation corresponds to the case where the soft internal layer is uncharged and supports a

8 negatively charged external soft layer. A further decrease in β_1 (< 0) comes to increase the

9 magnitude of the (now positive) charge carried by the innermost layer so that, in turn, $\Delta\varepsilon'(\omega)$

10 increases but to an extent that is lower as compared to the situation where internal and external soft

11 layers carry charges of the same sign. Inspection of the variations of $\varepsilon''(\omega)$ with ω reveals that the

12 characteristic frequency ω_α for the α-relaxation process does not depend on β_1, a result that is

13 according to expectation.

14   In Figure 2B, the background electrolyte concentration c^* is increased by a factor 10 as

15 compared to the situation depicted in panel A. For values of β_1 in the range $-2 \le \beta_1 \le 2$, $\Delta\varepsilon'(\omega)$

16 decreases in magnitude with increasing c^* (see comparison between Figures 2A and 2B). This

17 decrease is related to the screening of the fixed charges within the soft layers by ions from the

18 electrolyte solution, which leads to a reduction of the magnitude of the local equilibrium potential

19 throughout the soft bilayered interphase (see Figure S3 in Supporting Information). On the opposite,

20 $\Delta\varepsilon'(\omega)$ increases in magnitude with increasing c^* for $\beta_1 = -5$ and 5. In order to decipher the

21 mechanism responsible for this apparent non-monotonous variation of $\Delta\varepsilon'(\omega)$ with c^* and β_1, we

22 report in Figure 2C the quantity $\Delta\varepsilon'(\omega \to 0)$ as a function of c^* for various values of β_1 and $\lambda_2^0 d_2$.

23 At $\lambda_2^0 d_2 = 1$ (condition of Figures 2A, 2B) and low values of β_1, $\Delta\varepsilon'(\omega \to 0)$ continuously

24 decreases with increasing c^* and reaches zero value for $c^* > 100$ mM, a salt level that corresponds to

25 a complete screening of the charges located within the bilayered soft interphase. This trend is in line

26 with results of Figures 2A and 2B for low values of β_1. For sufficiently large values of β_1 ($\beta_1 = 5$),

27 $\Delta\varepsilon'(\omega)$ first increases with increasing c^* from 1 mM to *ca.* 4 mM and decreases upon further

28 increase of c^*. This maximum in $\Delta\varepsilon'(\omega)$, as anticipated from inspection of Figures 2A-2B for

29 $|\beta_1| = 5$, results from the polarisation of the particle EDL, a process that comes into play for

1   sufficiently large charge density (or $|\beta_1|$ value) within the soft component of the particle. This

2   polarization of the EDL results in the setting of an induced electric field that counteracts the effect

3   of the externally applied field. This leads in turn to a decrease of the dielectric permittivity. This

4   EDL polarization gradually vanishes upon increase of the field frequency because co- and counter-

5   ions have then not sufficient time to redistribute at the poles of the particle and thus create an

6   efficient counteracting polarization field. From the insert of Fig. 2B, it is further noted that ω_α does

7   not depend on c^*, which conforms to the expression of ω_α. Figures 2A and 2B reveal that the

8   charge of the internal layer of the considered soft interphase may substantially affect the dielectric

9   response of the particle as a whole. This important result cannot be recovered from standard

10   electrodynamic formalism where the interphase is represented in terms of a single polymeric layer

11   with given electrohydrodynamic properties.

12   In Figure 2D, we further underline the important contribution of the internal charged layer on

13   $\Delta\varepsilon'(\omega)$ by examining the impact of the flow penetration length scale as compared to the thickness

14   of the layer that directly faces the outer electrolyte solution. As the product $\lambda_2^0 d_2$ increases from 1

15   (Figure 2A) to 10 (Figure 2D) at fixed electrolyte concentration, the soft interphase becomes less

16   prone to electroosmotic flow intrusion. As a result, the spatial fraction of the interphase where ions

17   are active from an electrokinetic point of view is shifted toward the external region of the soft

18   interphase where electroosmotic flow velocity is largest, and this region is that where the local

19   electrostatic potential is lowest, as shown in Figure S3 (Supporting Information) for the equilibrium

20   regime ($\omega \to 0$). Accordingly, the limitation of the electroosmotic flow to probe internal charges of

21   the particle with increasing $\lambda_2^0 d_2$ is accompanied by a decrease in $\Delta\varepsilon'(\omega)$, which is in line with the

22   results displayed in Figure 2A and 2D. This trend is also reflected in the results of Figure 2C: the

23   larger $\lambda_2^0 d_2$, the lower the effective charge of the multilayered interphase, the lower $\Delta\varepsilon'(\omega \to 0)$,

24   and the less marked the polarization maximum. As expected, the examination of the frequency-

25   dependence of $\varepsilon''(\omega)$ in Figure 2D indicates that λ_2^0 has no impact on ω_α

26

27   **3.1.2. Dynamic mobility**

28   The counterparts of Figure 2 for the dynamic mobility are given in Figure 3. For the sake of

29   conciseness, we solely discuss in this section the dependence of the dimensionless real part of the

30   dynamic mobility, $\bar{\mu}'(\omega) = \mu_e'(\omega) e\eta / \varepsilon_0 \varepsilon_r k_B T$, on the applied field frequency.

1   In Figure 3A, the impact of β_1 on $\overline{\mu}'(\omega)$ is first examined for fixed c^* and $\lambda_2^0 d_2$ (c^* = 1mM and

2    $\lambda_2^0 d_2$ =1). Note that the adopted value of $\lambda_2^0 d_2$ is in line with a strong penetration of the

3   electroosmotic flow within the outer layer of soft multilayered interphase. This flow thus

4   significantly probes the electrostatic potential distribution within the internal layer 1 and is further

5   significantly affected by the magnitude of the frictional forces exerted by the polymer segments

6   therein. These two features intrinsically depend on β_1 and β_1^H (under the conditions of Figure 3,

7    $\beta_1^H = |\beta_1|$). For the cases examined in Figure 3A that correspond to $\beta_1 \geq 0$, both the inner and outer

8   layers carry negative charges (ρ_2^0 / F = -10 mM) and, as expected, the dynamic mobility is negative

9   over the entire range of ω. On the other hand, for $\beta_1 < 0$, the charge density within the inner layer is

10   positive and the results show that $\overline{\mu}'(\omega)$ then becomes positive despite of the negative charge

11   carried by the external layer where the electroosmotic flow is most significant. This feature can be

12   explained as follows. At c^* = 1 mM, the electric double layer thickness is larger than the thickness of

13   the outer surface layer of the particle (κd_2 < 1). In this thin double layer limit, the sign and

14   magnitude of the potential distribution all across the soft interphase are significantly (or entirely)

15   determined by the charge features of the inner layer (Figure S3, panel A). The sign of $\overline{\mu}'(\omega)$ is then

16   exclusively governed by the sign of the charge of the inner layer, a result that may be

17   counterintuitive if reasoning on the sole basis of the particle outer surface properties. In line with

18   this argument, $\overline{\mu}'(\omega)$ decreases with increasing β_1 from -5 to -1, thus following the corresponding

19   reduction in the positive potentials throughout the interphase, as illustrated in Figure S3 at low field

20   frequency. It should be kept in mind that increasing β_1 from -5 to -1 concomitantly leads to a

21   decrease of β_1^H, or equivalently, a decrease of the local friction exerted by the inner most polymer

22   segments on the flow. This latter effect should on its own contribute to increasing the particle

23   dynamic mobility, which is not observed. The electrostatic contribution of the innermost layer then

24   overwhelms the expected hydrodynamic impact of this layer on the dynamic mobility of the particle

25   as a whole. The situation obviously changes with increasing β_1 from 0 to 5, *i.e.* with increasing the

26   magnitude of the negative charge of the innermost layer of the soft interphase. In agreement with

27   preceding arguments, the dynamic mobility is negative and it increases in absolute value for

28   increasing β_1 from 0 to 1 over the entire range of ω tested (electrostatic effect). However, with

29   further increasing β_1 from 1 to 5, the results show that $|\overline{\mu}'(\omega)|$ decreases at low frequency (typically

1   $< 10^7$ s^{-1}) after passing a maximum, whereas it increases at large frequency ($> 10^7$ s^{-1}). In the latter

2   regime, ω is above the characteristic frequency ω_{MWO} of the Maxwell-Wagner-O'Konski

3   (MWO) relaxation process ($\omega_{MWO}/2\pi = \kappa^{-2}/2\pi(D_+ + D_-) \approx 3.10^6$ s^{-1} with $c^* = 1$ mM and $D_+ = D_- =$

4   10^{-9} m^{2}s^{-1})[45, 46], so that there is no sufficient time for the counterions to diffuse/migrate across the

5   EDL (MWO relaxation results from the accumulation of counterions on one side of the particle and

6   the depletion on the other side due to the migration/diffusion of these ions throughout the EDL)[45,

7   46]. At frequencies larger than ω_{MWO}, there is no significant polarization of the EDL and generation

8   of an induced-electric field that counteracts the action of the externally applied field. As a result, the

9   dynamic mobility simply increases in magnitude at large frequency with increasing the charge

10 density of the inner layer. In the former regime where ω is below ω_{MWO}, the aforementioned induced

11 electric field is created, pointing against the applied field, so that the dynamic mobility decreases

12 with increasing β_1. In turn, $\overline{\mu}'(\omega)$ passes through a maximum with increasing β_1 from 0 to 5 at

13 fixed low frequency as the result of the accompanied polarization process. It should also be

14 mentioned that, at frequencies above 10^7 s^{-1}, all the curves display a continuous decrease in

15 magnitude of $\overline{\mu}'(\omega)$ as ω increases. Indeed the frequency is so high, $\omega > \omega_i$ with $\omega_i = 2\eta/\rho_m a^2$,

16 that the inertia of the fluid and the particle hinders motion.[45, 46] For $\beta_1 = -5$ and 5, the curves $\overline{\mu}'(\omega)$

17 are shaped both by the MWO and α relaxations, which is manifested by the presence of an

18 extremum. With increasing β_1 in intermediate values, $|\overline{\mu}'(\omega)|$ monotonously decreases over the

19 whole range of ω. This feature is caused by the decrease in the magnitude of the electrostatic

20 potentials probed by the hydrodynamic flow as $|\beta_1|$ decreases (see Figure S3, Supporting

21 Information).

22   The effect of background electrolyte concentration c^* on the dynamic mobility is provided by

23 the comparison between results collected in Figure 3A ($c^* = 1$ mM) and in Figure 3B ($c^* = 10$ mM).

24 Obviously, increasing c^* not only results in the expected decrease of $|\overline{\mu}'(\omega)|$ following particle

25 charge screening (situation met for $\beta_1 = -2, 0, 1$) but it may also lead to a reversal of the mobility

26 sign (cases $\beta_1 = -1$), an increase of its magnitude (cases $\beta_1 = -5, 5$) or even leave basically

27 unchanged the value of the dynamic mobility (case $\beta_1 = 2$). Let us discuss these three latter results.

28   First, consider the cases $\beta_1 = -5, 5$. In order to properly understand the corresponding trend in

29 $\overline{\mu}'(\omega)$, we showed in Figure 3C, the variations of $\overline{\mu}'(\omega \to 0)$ as a function of c^* for various values

1   of β_1 and $\lambda_2^0 d_2$. At $\lambda_2^0 d_2 = 1$ and $\beta_1 = 5$, the magnitude of $\bar{\mu}'(\omega \to 0)$ increases upon increase of c^*

2   from 1 mM, grows through a maximum at *ca.* 40 mM and finally decreases to a nonzero value (not

3   shown here), which is characteristic of the presence of a soft layer that carries a given volume

4   charge density.[2] As previously reported, an EDL polarization occurs for sufficiently high

5   magnitudes of electrostatic potentials across the interphase. This polarization then gives rise to an

6   induced electric field that points against the externally applied field and hence tends to hinder the

7   motion of the particles. As c^* increases from 1 mM to *ca.* 40 mM, the decreasing magnitudes in the

8   potential distributions weakens the EDL polarization. As a result, $\bar{\mu}'(\omega \to 0)$ increases. For $\beta_1 = 2$,

9   the magnitude of the dynamic mobility over the entire range of ω is not significantly affected by the

10   increase of c^* from 1 to 10 mM. This feature is also reflected in Figure 3C. Consider the situation

11    $\lambda_2^0 d_2 = 1$ and $\beta_1 = 2$. The curve shows that the magnitudes of $\bar{\mu}'(\omega \to 0)$ at $c^* = 1$ and 10 mM are

12   approximately the same. However the magnitude of $\bar{\mu}'(\omega \to 0)$ is not constant in this range of c^*

13   but it slightly increases with the increase of c^* from 1 to 3 mM (explanation above in the text) and

14   then gradually decreases. In the last situation $\beta_1 = -1$, increasing c^* from 1 to 10 mM leads to a

15   change of the mobility sign over the entire range of ω (Figure 3B). In order to understand this trend,

16   we reported in Figure 4 $\bar{\mu}'(\omega \to 0)$ as a function of c^*. $\bar{\mu}'(\omega \to 0)$ is positive at $c^* = 1$ mM, it

17   gradually decreases upon increase of c^* and becomes negative at $c^* \approx 2$ mM before reaching a

18   negative constant value for $c^* > 20$ mM. At $c^* < 2$ mM, the Debye length is larger than the thickness

19   of the outer layer 2 ($\kappa d_2 < 1$). As a result, the magnitude and sign of the potential distribution across

20   the interphase and, consequently, of the mobility are mostly governed by the electrohydrodynamic

21   properties of the inner layer. On the opposite, as c^* increases from 2 mM, the EDL becomes thinner

22   than the outer layer ($\kappa d_2 > 1$). $\bar{\mu}'(\omega \to 0)$ is then increasingly determined by the

23   electrohydrodynamic features of the most external layer 2.

24   We examine the effect of the electroosmotic flow penetration length within the soft interphase

25   *via* the increase of the parameter $\lambda_2^0 d_2$ from 1 (Figure 3A) to 10 (Figure 3D). As $\lambda_2^0 d_2$ increases,

26   the electroosmotic flow penetration becomes limited. As a result the electroosmotic flow probes

27   decreasing magnitudes of local potentials (as shown by Figure S3). Hence, at a given β_1 and

28   electrolyte concentration, the magnitude of the dynamic mobility is expected to decrease, which is

29   indeed observed from the comparison of Figures 3A and 3D. This trend is also illustrated in Figure

30   3C. The increase of $\lambda_2^0 d_2$ comes along with the decrease of $\bar{\mu}'(\omega \to 0)$ and the disappearance of

1   the maximum marking EDL polarization. From Figure 3C, consider the situation of a poor flow

2   penetration length (*i.e.* $\lambda_2^0 d_2$ = 10). In this situation the flow penetration is too limited for

3    $\bar{\mu}'(\omega \to 0)$ to depend on the charge and friction properties of the inner layer. As a result,

4    $\bar{\mu}'(\omega \to 0)$ becomes quasi-independent of β_1 over the entire range of ionic strengths considered.

5   Finally, Figure 3A shows that the curves $\bar{\mu}'(\omega)$ are shaped by both α and MWO relaxations for

6   β_1 = -5 and 5. However the resulting extremum (at $\omega \approx \omega_{MWO}$) is less pronounced for increasing

7   values of c^* (Figure 3B) and decreasing flow penetration length (Figure 3D) because of decreasing

8   magnitudes in the potential distributions probed by the electroosmotic flow (see Figure S3,

9   Supporting Information).

10

11   **3.2. Impact of the thickness of the soft layers on the dynamic mobility**

12   Figure 5 displays the dependence of $\bar{\mu}'(\omega)$ on the ratio between thicknesses of external and

13   internal layers, d_2/d_1, under various conditions of salt concentrations in the range 1 mM to 50 mM

14   for situations of poor to large flow penetration lengths within the outer layer ($1/\lambda_2^0$ =0.1 nm in panel

15   A-C, and $1/\lambda_2^0$ =5 nm in panels D-F). For all cases tested, the overall thickness of the soft bilayered

16   shell is maintained constant (d_1+d_2 = 30 nm), the charge density of layer 2 and 1 are negative and

17   positive, respectively, with ρ_2^0 / F = -10 mM and β_1 = -5.

18   Let us first examine Figures 5A-C where $1/\lambda_2^0$ =0.1 nm. At low ionic strength (c^* = 1 mM, Fig.

19   5A) and for $d_2/d_1 \to \infty$, $\bar{\mu}'(\omega)$ is solely determined by the electrohydrodynamic features of the

20   outermost layer 2 and accordingly $\bar{\mu}'(\omega)$ is negative over the entire range of frequency. In the other

21   extreme $d_2/d_1 \to 0$, $\bar{\mu}'(\omega)$ is positive and is determined by the charged and friction properties of the

22   inner layer 1 of the soft interphase. With increasing d_2/d_1 from 0 to 0.2, $\bar{\mu}'(\omega)$ decreases without

23   changing sign. This decrease in dynamic mobility is due to the impact of the negatively charged

24   layer 2 on the electrostatic potential distribution across the positively charged layer 1. For d_2/d_1

25   varying between 0 to 0.2, the Debye length remains larger than d_2 and the second layer then

26   effectively leads to a decrease in the potential within layer 1 (see Figure S4, Supporting

27   Information) and thus to that of $\bar{\mu}'(\omega)$. An additional increase in d_2/d_1 causes a change in the sign

28   of the potential because the thickness of layer 2 then becomes appreciable as compared to $1/\kappa$. In

1   turn, this is reflected by change in sign of dynamic mobility. In those situations, $\bar{\mu}'(\omega)$ becomes

2   increasingly determined by the electrohydrodynamic properties of layer 2 and for d_2/d_1 values larger

3   than 5 (which correspond to large $\kappa d_2 \approx 5$), the magnitude and the sign of $\bar{\mu}'(\omega)$ are exclusively

4   fixed by the properties of layer 2. For $d_2/d_1 = 0$, the curve $\bar{\mu}'(\omega)$ displays a maximum that results

5   from the MWO relaxation. However, as d_2/d_1 increases, this maximum becomes less pronounced

6   ($d_2/d_1 = 0.2$) and even completely disappears with further increase of the ratio d_2/d_1. This trend is

7   similar to that obtained in section 3.1.2 and results from the decrease in the local electrostatic

8   potentials probed by the electroosmotic flow as d_2/d_1 increases (as shown by Figure S4).

9   With increasing c^* at a given ratio d_2/d_1 (Figures 5A to 5C), the electric double layer with its

10   accompanied strong electric field becomes mainly located within the outermost region of the

11   bilayered interphase. The impact of the internal layer 1 on the dynamic mobility then becomes less

12   and less pronounced. This is in line with Figures 5A-5C which shows how the mobility may change

13   sign at fixed d_2/d_1 with increasing c^* as a result of the associated modifications of the respective

14   contributions of layers 1 and 2 to $\bar{\mu}'(\omega)$. This feature together with the extent of screening of the

15   interphasial charge by electrolyte ions explain the dependence of the magnitude and sign of $\bar{\mu}'(\omega)$

16   on c^* and d_2/d_1.

17   The effect of the flow penetration length c^* on $\bar{\mu}'(\omega)$ is shown by the comparison between the

18   results displayed in the Figure 5A-C ($1/\lambda_2^0 =0.1$ nm) and Figure 5D-E ($1/\lambda_2^0 =5$ nm). For $1/\lambda_2^0 = 5$

19   nm, the overall variations of $\bar{\mu}'(\omega)$ for various d_2/d_1 ratios and electrolyte concentrations c^* are

20   very similar to those detailed in the case $1/\lambda_2^0 = 0.1$ nm. However, at a given c^*, the charge and

21   friction properties of the inner layer increasingly govern the sign and magnitude of $\bar{\mu}'(\omega)$ upon

22   increase of $1/\lambda_2^0$. On one hand, for $1/\lambda_2^0 = 0.1$ nm and $d_2/d_1 > 0$, $\bar{\mu}'(\omega)$ is solely determined by the

23   electrohydrodynamic properties of the outer layer at $c^* = 50$ mM (see Figure 5C). On the other

24   hand, for $1/\lambda_2^0 = 5$ nm, it is necessary to further increase the electrolyte concentration in order to

25   hinder completely the contribution of layer 1 (as shown by Figure 5F). This trend results from the

26   larger penetration flow length scale in the soft layers, which enhances the contribution of the inner

27   layer to dynamic mobility. Finally, Figure 5D shows that the curves $\bar{\mu}'(\omega)$ are shaped by both α

28   and MWO relaxations for $d_2/d_1 = 0$ and 0.2, resulting in the apparition of a maximum at $\omega \approx \omega_{MWO}$.

1   This maximum is more pronounced for $1/\lambda_2^0 = 5$ nm than for $1/\lambda_2^0 = 0.1$ nm because of the larger

2   potential distributions probed by the electroosmotic flow. As previously discussed, the maximum

3   gradually disappears upon further increase of d_2/d_1 and/or c^*.

4   Note that we do not discuss here the dielectric spectra under conditions of Figure 5. The

5   variations of $\Delta\varepsilon'(\omega)$ follows indeed the variations in the total charge as discussed before. We

6   systematically verified that ω_α is independent of d_2/d_1 and $d_1 + d_2$ regardless of the permeability of

7   the constituting soft layers.

8

9   **3.3. Effect of the spatial distribution of fixed charges within the soft layers**

10   In this section, we discuss the impact of a heterogeneous spatial distribution of fixed charges

11   within a given layer on $\bar{\mu}'(\omega)$. As detailed in Section 2.1, this heterogeneity is described by the

12   parameters $\alpha_{i=1,2}$. The dependence of $\bar{\mu}'(\omega)$ on frequency $\omega/2\pi$ is provided in Figure 6A for three

13   sets of parameters $\alpha_{i=1,2}$. We further adopted the following model parameters: $c^*=10$ mM, $\rho_2^0/F = $ -

14   20 mM, $\beta_1 =-2$ and $\lambda_2^0 d_2 =2$. The corresponding potential spatial distributions and charge density

15   profiles across the interphase are given in Figure 6B and Figure 6C, respectively. In Figure 6B, the

16   dotted lines represents the boundaries between layer 1/layer 2 and layer 2/solution in the limit $\alpha_{i=1,2}$

17   $\rightarrow$0. From Figure 6A, the results show a slight increase in magnitude of $\bar{\mu}'(\omega)$ as α_2 increases from

18   0 to 5 nm while α_1 is kept unchanged. In order to understand this trend, consider the corresponding

19   potential distributions in panel B. The flow penetration length being smaller than the thickness of

20   the outer layer ($\lambda_2^0 d_2 =2$), the electroosmotic flow probes increasingly large local electrostatic

21   potentials upon increase of α_2, thus leading to the observed increase in magnitude of the mobility.

22   However the motion of the particle is also partially hindered by a hydrodynamic effect: the polymer

23   segments protuding toward the outer solution lead to an increase in the local friction experienced by

24   the flow. This is the reason why $\bar{\mu}'(\omega)$ only slightly increases in magnitude with increasing α_2 at

25   fixed α_1. Increasing α_1 from 0 to 5 nm leads to a reduction in the local potential within the outer

26   soft corona region that is significantly probed by the flow (see panel B) and to an increase of the

27   local friction exerted by the polymer segments. Both of these features lead to a decrease in the

28   magnitude of the mobility, which is indeed observed. Obviously, disregarding the diffuseness in the

29   spatial distributions of fixed charges within a given layer may lead to an over- or under-estimation

1   in the magnitude of the dynamic mobility at a given frequency and thus to a mis-interpretation of

2   experimental data. It is further recalled that the thickness and diffuseness of the corona of soft

3   interphase, whether multilayered or not, are inherently depending on solution ionic strength (via

4   swelling processes), which has dramatic implications in terms of DC electrokinetic response and

5   data interpretation.[33, 47] The current formalism allows for tackling these complex heterogeneity

6   issues using AC electrokinetic experiments.

7   The dielectric spectra are not shown here. The introduction of the parameter χ in eqn (4)

8   ensures a constant amount of charges (Q_{tot}) across the soft interface upon variation of $\alpha_{i=1,2}$. In

9   agreement with the results obtained in section 3.1.1, neither the magnitude of $\Delta\varepsilon'(\omega)$ nor ω_α are

10 significantly affected by the variations in $\alpha_{i=1,2}$.

11

12 **3.4. Effect of the number of soft layers N in the multi-layered interphase**

13   In the following, we consider a suspension of particles covered by N concentric soft layers of

14 thicknesses $d_i = d_{i+1}$. The variations of $\Delta\varepsilon'(\omega)$ and $\bar{\mu}'(\omega)$ with $\omega/2\pi$ are determined for various

15 values of N (from 1 to 5) while the total charge and total thickness of the soft interphase remain

16 constant (Figure 7A). In details, we consider soft interphases satisfying $\beta_{i=1\ldots N} = N - i + 1$. For

17 illustration, the spatial distributions of $\rho_{fix}(x)/F$ throughout the soft interphase for various $N=1,\ldots,5$

18 are displayed in Figure 7A. The corresponding equilibrium potential distributions are shown in

19 Figure 7B. The variations in $\Delta\varepsilon'(\omega)$ with $\omega/2\pi$ are then reported as a function N for two different

20 values of flow penetration lengths, *i.e.* $1/\lambda_N^0 \to 0$ (Figure 8A, impermeable case) and $1/\lambda_N^0 = 5$ nm

21 (Figure 8B, permeable case). In the situation of an impermeable particle, *i.e.* $1/\lambda_N^0 \to 0$, the increase

22 of N does not impact the dielectric response of the system. In order to understand this feature,

23 consider the corresponding potential distributions displayed in Figure 7B. For $1/\lambda_N^0 \to 0$, the

24 electroosmotic flow probes the local electrostatic potential distribution outside the soft layers ($\kappa(r-$

25 $a) > 2.6$). In this spatial region, the discrepancies between the various potential profiles upon

26 increase of N are limited. As a result, they do not lead to significant variations between the

27 corresponding dielectric spectra. This feature is in line with the fact that the permittivity mostly

28 depends on the amount of fixed charges Q_{tot}, which is kept constant upon increase of N. However,

29 the situation changes upon increase of $1/\lambda_N^0$ from 0 to 5 nm. Figure 8B shows that the magnitude

30 of $\Delta\varepsilon'(\omega)$ slightly decreases as N increases for frequencies below ω_α ($\omega_\alpha/2\pi \approx 5.10^3$ s^{-1}), while it

1   remains constant for $\omega > \omega_\alpha$. Let us comment on these two trends. First consider the potential

2   distribution reported in Figure 7B. For $1/\lambda_N^0$ = 5nm, the electroosmotic flow significantly

3   penetrates within the soft layers as N increases and the magnitude of $\Delta\varepsilon'(\omega)$ decreases for $\omega < \omega_\alpha$,

4   following the decrease in the magnitude of the outer potential distribution with increasing N (Figure

5   7B) For $\omega > \omega_\alpha$, the co- and counter-ions have not sufficient time to diffuse/migrate at the sides of

6   the particles so that the dielectric response remains constant upon variations of N. The dependence

7   of $\bar{\mu}'(\omega)$ on $\omega/2\pi$ for various values of N is illustrated in panel C ($1/\lambda_N^0 \to 0$) and D ($1/\lambda_N^0$ =5 nm).

8   In both situations, $\bar{\mu}'(\omega)$ decreases in magnitude as N increases. Indeed, the examination of Figure

9   7B shows a decrease of the local potential upon increase of N in the spatial region that is accessible

10   by the electroosmotic flow. As expected from the results obtained in section 3.1, the number of

11   layers N impacts more significantly the magnitude of $\bar{\mu}'(\omega)$ than that of $\Delta\varepsilon'(\omega)$. The dielectric

12   permittivity is mainly controlled by the total charge carried by the soft interphase (kept constant in

13   this study), while the mobility is more affected by the friction properties and local electrostatic

14   potentials probed by the electroosmotic flow. Finally, these results clearly prove that reducing a

15   multilayered interphase to a monolayer interphase with the same total charge may lead to an

16   over/under-estimation in the magnitude of the dynamic mobility, especially in the low frequency

17   range.

18

19

20

21   **4.   Conclusions**

22   In this theoretical study, the frequency dependence of the dynamic mobility and dielectric

23   permittivity of suspensions of soft diffuse multi-layered (bio)particles is examined. The impacts of

24   the key electrohydrodynamic features defining the constituting soft layers of the whole polymeric

25   corona of the particles are detailed. In particular, it is shown how the electrostatic and

26   hydrodynamic properties of the inner layers affect the magnitude of the frequency-dependent

27   permittivity, and the magnitude and sign of the frequency-dependent dynamic mobility especially at

28   low ionic strengths and large particle hydrodynamic permeabilities. These conditions indeed

29   correspond to those where electric double layer extension and flow field distributions within the

30   particle are significantly governed by the electrohydrodynamic features of the internal shell layers.

31   This theoretical study extends previous models strictly applicable to AC electrodynamics of soft

1   monolayered particles. It constitutes a necessary guide for understanding the electrodynamic

2   characteristics of complex soft multi-layered particles such as bacteria, viruses or synthetic

3   polyelectrolyte microgel particles from AC electrodynamic techniques.

4

5

6   **References**

7

8   1.   J. F. L. Duval and F. Gaboriaud, *Current Opinion in Colloid & Interface Science*, 2010, 15,
9   184-195.
10   2.   H. Ohshima, *Advances in Colloid and Interface Science*, 1995, 62, 189-235.
11   3.   J. F. L. Duval and H. Ohshima, *Langmuir*, 2006, 22, 3533-3546.
12   4.   J. F. L. Duval, R. Zimmermann, A. L. Cordeiro, N. Rein and C. Werner, *Langmuir*, 2009,
13   25, 10691-10703.
14   5.   R. J. Hill, D. A. Saville and W. B. Russel, *Journal of Colloid and Interface Science*, 2003,
15   258, 56-74.
16   6.   D. A. Saville, *Journal of Colloid and Interface Science*, 2000, 222, 137-145.
17   7.   J. F. L. Duval, H. J. Busscher, B. van de Belt-Gritter, H. C. van der Mei and W. Norde,
18   *Langmuir*, 2005, 21, 11268-11282.
19   8.   F. Gaboriaud, M. L. Gee, R. Strugnell and J. F. L. Duval, *Langmuir*, 2008, 24, 10988-
20   10995.
21   9.   G. Francius, P. Polyakov, J. Merlin, Y. Abe, J.-M. Ghigo, C. Merlin, C. Beloin and J. F. L.
22   Duval, *PLoS ONE*, 2011, 6, e20066.
23   10.   J. Langlet, F. Gaboriaud, C. Gantzer and J. F. L. Duval, *Biophysical Journal*, 2008, 94,
24   3293-3312.
25   11.   J. J. López-García, C. Grosse and J. Horno, *Journal of Colloid and Interface Science*, 2003,
26   265, 327-340.
27   12.   C. Dika, J. F. L. Duval, H. M. Ly-Chatain, C. Merlin and C. Gantzer, *Appl. Environ.*
28   *Microbiol.*, 2011, 77, 4939-4948.
29   13.   J. Lyklema, H. P. van Leeuwen and M. Minor, *Advances in Colloid and Interface Science*,
30   1999, 83, 33-69.
31   14.   J. Merlin and J. F. L. Duval, *Physical Chemistry Chemical Physics*, 2012.
32   15.   C. S. Mangelsdorf and L. R. White, *Journal of the Chemical Society, Faraday Transactions*,
33   1992, 88, 3567-3581.
34   16.   C. S. Mangelsdorf and L. R. White, *Journal of Colloid and Interface Science*, 1993, 160,
35   275-287.
36   17.   H. Ohshima, *Journal of Colloid and Interface Science*, 1996, 179, 431-438.
37   18.   J. Ennis and L. R. White, *Journal of Colloid and Interface Science*, 1996, 178, 446-459.
38   19.   F. Carrique, A. Quirantes and A. V. Delgado, *Colloids and Surfaces A: Physicochemical*
39   *and Engineering Aspects*, 1995, 97, 141-149.
40   20.   F. Carrique, *Journal of Chemical Physics*, 2003, 118, 1945-1956.
41   21.   R. J. Hill, *Physical Chemistry Chemical Physics*, 2003, 5, 911-915.
42   22.   F. J. Arroyo, F. Carrique, S. Ahualli and A. V. Delgado, *Physical Chemistry Chemical*
43   *Physics*, 2004, 6, 1446-1452.
44   23.   B. H. Bradshaw-Hajek, S. J. Miklavcic and L. R. White, *Langmuir*, 2008, 24, 4512-4522.
45   24.   B. H. Bradshaw-Hajek, S. J. Miklavcic and L. R. White, *Langmuir*, 2009, 25, 1961-1969.

1   25.   R. J. Hill, D. A. Saville and W. B. Russel, *Journal of Colloid and Interface Science*, 2003,
2   268, 230-245.
3   26.   R. J. Hill, D. A. Saville and W. B. Russel, *Journal of Colloid and Interface Science*, 2003,
4   263, 478-497.
5   27.   J. J. López-García, C. Grosse and J. Horno, *Journal of Colloid and Interface Science*, 2003,
6   265, 341-350.
7   28.   S. Ahualli, M. L. Jiménez, F. Carrique and A. V. Delgado, *Langmuir*, 2009, 25, 1986-1997.
8   29.   C. Cametti, *Soft Matter*, 2011, 7, 5494-5506.
9   30.   S. Uppapalli and H. Zhao, *Langmuir*, 2012, 28, 11164-11172.
10 31.   T. G. Mason and M. Y. Lin, *Physical Review E - Statistical, Nonlinear, and Soft Matter
11   Physics*, 2005, 71, 040801/040801-040801/040804.
12 32.   A. Fernández-Nieves, F. J. De las Nieves and A. Fernández-Barbero, *Journal of Chemical
13   Physics*, 2004, 120, 374-378.
14 33.   R. Zimmermann, S. S. Dukhin, C. Werner and J. F. L. Duval, *Current Opinion in Colloid &
15   Interface Science*, 2013, 18, 83-92.
16 34.   J. F. L. Duval, D. Küttner, C. Werner and R. Zimmermann, *Langmuir*, 2011, 27, 10739-
17   10752.
18 35.   C. N. Rochette, J. J. Crassous, M. Drechsler, F. Gaboriaud, M. Eloy, B. de Gaudemaris and
19   J. F. L. Duval, *Langmuir*, 2013, 29, 14655-14665.
20 36.   J. F. L. Duval, J. Merlin and P. A. L. Narayana, *Physical Chemistry Chemical Physics*,
21   2010, 13, 1037-1053.
22 37.   T. P. Russel, *Materials Science Reports*, 1990, 5, 171-271.
23 38.   S. H. Anastasiadis, T. P. Russel, S. K. Satija and C. F. Majkrzak, *The Journal of Chemical
24   Physics*, 1990, 92, 5677-5691.
25 39.   A. Budkowski, *Advances in Polymer Science*, Berlin Heidelberg, 1999.
26 40.   S. Kuwabara, *Journal of the Physical Society of Japan*, 1959, 14, 527-532.
27 41.   S. Ahualli, A. Delgado, S. J. Miklavcic and L. R. White, *Langmuir*, 2006, 22, 7041-7051.
28 42.   R. W. O'Brien, A. Jones and W. N. Rowlands, *Colloids and Surfaces A: Physicochemical
29   and Engineering Aspects*, 2003, 218, 89-101.
30 43.   S. Ahualli, A. V. Delgado, S. J. Miklavcic and L. R. White, *Journal of Colloid and Interface
31   Science*, 2007, 309, 342-349.
32 44.   M. A. Preston, R. Kornbrekke and L. R. White, *Langmuir*, 2005, 21, 9832-9842.
33 45.   C. Grosse and A. V. Delgado, *Current Opinion in Colloid and Interface Science*, 2010, 15,
34   145-159.
35 46.   V. N. Shilov, A. V. Delgado, F. González-Caballero, J. Horno, J. J. López-García and C.
36   Grosse, *Journal of Colloid and Interface Science*, 2000, 232, 141-148.
37 47.   R. Zimmermann, D. Kuckling, M. Kaufmann, C. Werner and J. F. L. Duval, *Langmuir*,
38   2010, 26, 18169-18181.
39

40 **Figures captions**

41

42 **Figure 1.**   (Panel A) Schematic representation of a soft multi-layered spherical particle consisting

43   of a hard core covered by N concentric soft polymeric layers and subjected to an ac

44   electric field $\vec{E}(\omega)$. The figure details the spatial coordinates (r, θ) and the

45   nomenclature adopted for layers indexing. (Panel B) Schematic drawing of a

1 homogeneous (broken line) and a diffuse (solid line) spatial distribution of polymer

2 segments throughout the interphase. d_i corresponds to the thickness of layer i, a is the

3 particle core radius, $\beta_i = \rho_i^0 / \rho_N^0$ is the ratio between the density of charges carried by

4 layer i and that of charges carried by layer N, λ_i is the hydrodynamic softness of layer

5 i in the limit of a homogeneous distribution of polymer segments. α_i represents the

6 typical length over which the polymer segment density within layer i deviates from the

7 homogeneous case. The plain lines refer to diffuse distribution of polymer segments

8 and the dotted lines to step-function representation of the interfaces between layer i

9 and layer $i+1$. (Panel C) Illustration of a concentrated suspension of multilayered

10 particles according to Kuwabara's cell model.

11

12 **Figure 2.** (Panel A-C) Variations of dielectric increment $\Delta\varepsilon'$ and dielectric loss ε'' (insets) as a

13 function of field frequency $\omega / 2\pi$ for various ratios $\beta_1 = \rho_1^0 / \rho_2^0$ (indicated) with $c^* =$

14 1 mM and $\lambda_2^0 d_2 = 1$ (panel A); $c^* = 10$ mM and $\lambda_2^0 d_2 = 1$ (panel B) and $c^* = 1$ mM

15 and $\lambda_2^0 d_2 = 10$ (panel C). (Panel D) Variations of the magnitude of $\Delta\varepsilon'(\omega \to 0)$ as a

16 function of c^* for various ratios β_1 and $\lambda_2^0 d_2$ (indicated). Other parameters if not

17 indicated in Table 1: $\rho_2^0 / F = -10$mM; $d_1 = 20$nm; $d_2 = 5$nm; $a = 300$nm; $\phi = 0.01$;

18 $\alpha_{1,2} \to 0$; $z = 1$; $\beta_1^{\mathrm{H}} = |\beta_1|$.

19

20

21 **Figure 3.** (Panel A-C) Variations of dimensionless dynamic mobility $\overline{\mu}'$ as a function of field

22 frequency $\omega / 2\pi$ for various ratios β_1 (indicated) with $c^* = 1$ mM and $\lambda_2^0 d_2 = 1$

23 (panel A); $c^* = 10$ mM and $\lambda_2^0 d_2 = 1$ (panel B) and $c^* = 1$ mM and $\lambda_2^0 d_2 = 10$ (panel

24 C). (Panel D) Variations of the magnitude of the dimensionless electrophoretic

25 mobility $\overline{\mu}'(\omega \to 0)$ as a function of c^* for various ratios β_1 and $\lambda_2^0 d_2$ (indicated).

26 Other parameters if not indicated in Table 1: $\rho_2^0 / F = -10$mM; $d_1 = 20$nm; $d_2 = 5$nm;

27 $a = 300$nm; $\phi = 0.01$; $\alpha_{1,2} \to 0$; $z = 1$; $\beta_1^{\mathrm{H}} = |\beta_1|$.

28

1   **Figure 4.**   Variations of $\bar{\mu}'(\omega \to 0)$ as a function of c^* with $\beta_1 = 1$ $\lambda_2^0 d_2 = 1$. Other parameters if

2   not indicated in Table 1: $\rho_2^0 / F = -10$mM; $d_1 = 20$nm; $d_2 = 5$nm; $a = 300$nm; $\phi = $

3   0.01; $\alpha_{1,2} \to 0$; $z = 1$; $\beta_1^H = |\beta_1|$.

4

5   **Figure 5.**   Variations of dimensionless dynamic mobility $\bar{\mu}'$ as a function of field frequency $\omega /$

6   2π for various ratios d_2 / d_1 (indicated). (Panels A-C) Particles with hydrodynamic

7   Brinkman length $1 / \lambda_2^0 = 0.1$ nm are dispersed in a medium of concentration $c^* = 1$

8   mM (panel A), $c^* = 10$ mM (panel B) and $c^* = 50$ mM (panel C). (Panels D-F)

9   Particles with hydrodynamic Brinkman length $1 / \lambda_2^0 = 5$ nm are dispersed in a medium

10   of electrolyte concentration $c^* = 1$ mM (panel D), $c^* = 10$ mM (panel E) and $c^* = 50$

11   mM (panel F). Other parameters if not indicated in Table 1: $\rho_2^0 / F = -10$mM; $\beta_1 = -5$;

12    $d_1 + d_2 = 30$nm; $a = 300$nm; $\phi = 0.01$; $\alpha_{1,2} \to 0$; $z = 1$; $\beta_1^H = |\beta_1|$.

13

14   **Figure 6.**   (Panel A) Variations of dimensionless dynamic mobility $\bar{\mu}'$ as a function of field

15   frequency $\omega / 2\pi$ for various parameters α_i (indicated). Corresponding dimensionless

16   potential distribution (panel B) and corresponding charge density distribution (panel

17   C) throughout the interphase. The magnitude of the charge density in panel C gives an

18   indication of the variations of the normalized friction parameter $k(r) / k_N^o$ (see eqns (1-

19   2) and (5-6) with $\beta_1^H = |\beta_1|$). Other parameters if not indicated in Table 1: $c^* = 10$

20   mM; $\rho_2^0 / F = -20$mM; $\beta_1 = -2$; $\lambda_2^0 d_2 = 2$; $d_1 = 20$nm; $d_2 = 10$nm; $a = 300$nm; $\phi = 0.01$;

21    $z = 1$; $\beta_1^H = |\beta_1|$.

22

23   **Figure 7.**   Fixed charge density distribution (panel A) and dimensionless potential distribution

24   (panel B) throughout the interphase of particles covered by N=1 to N=5 polymer layers

25   (indicated). The total charge and thickness of the polymer shell remain constant upon

26   variation of N with $\sum_i d_i = 25$ nm. Other parameters if not indicated in Table 1: $c^* = $

27   1 mM; $a = 300$nm; $\phi = 0.01$; $\alpha_i \to 0$; $z = 1$; $\beta_i^H = |\beta_i|$.

28

1   **Figure 8.**   Variations of dielectric increment $\Delta\varepsilon'$ (panels A-B) and dimensionless dynamic

2   mobility $\bar{\mu}'$ (panels C-D) as a function of field frequency $\omega/2\pi$. The particles consist

3   of a hard core covered by N polymer layers (indicated) with various hydrodynamic

4   softness: $1/\lambda_N^0 \to 0$ (panel A and C) and $1/\lambda_2^0 = 5$nm (panels B and D). Other

5   parameters if not indicated in Table 1: $c^* = 1$ mM; $a = 300$nm; $\phi = 0.01$; $\alpha_i \to 0$; $z =$

6   1; $\beta_i^H = |\beta_i|$. The equilibrium fixed charge density and potential distribution

7   corresponding to the adopted multilayered interphase are given in Figures 7B and 7C,

8   respectively.

9

10

11   **Table 1.**   Electric and fluid dynamic data used for all calculations.

Temperature	$T = 298$ K
Relative permittivity of medium	$\varepsilon_r = 78.54$
Relative permittivity of hard core	$\varepsilon_p = 2.0$
Medium viscosity	$\eta = 0.954 \times 10^{-3}$ Pa s
Medium density	$\rho_m = 0.997$ g cm^{-3}
Hard core density	$\rho_p = 1.05$ g cm^{-3}
Charge surface of hard core	$\sigma_s = 0$ C m^{-2}
Limiting conductance of cation K$^+$	$\Lambda_+^o = 7.35 \times 10^{-3}$ S m^{2}mol^{-1}
Limiting conductance of anion NO$_3^-$	$\Lambda_-^o = 7.146 \times 10^{-3}$ S m^{2}mol^{-1}

12
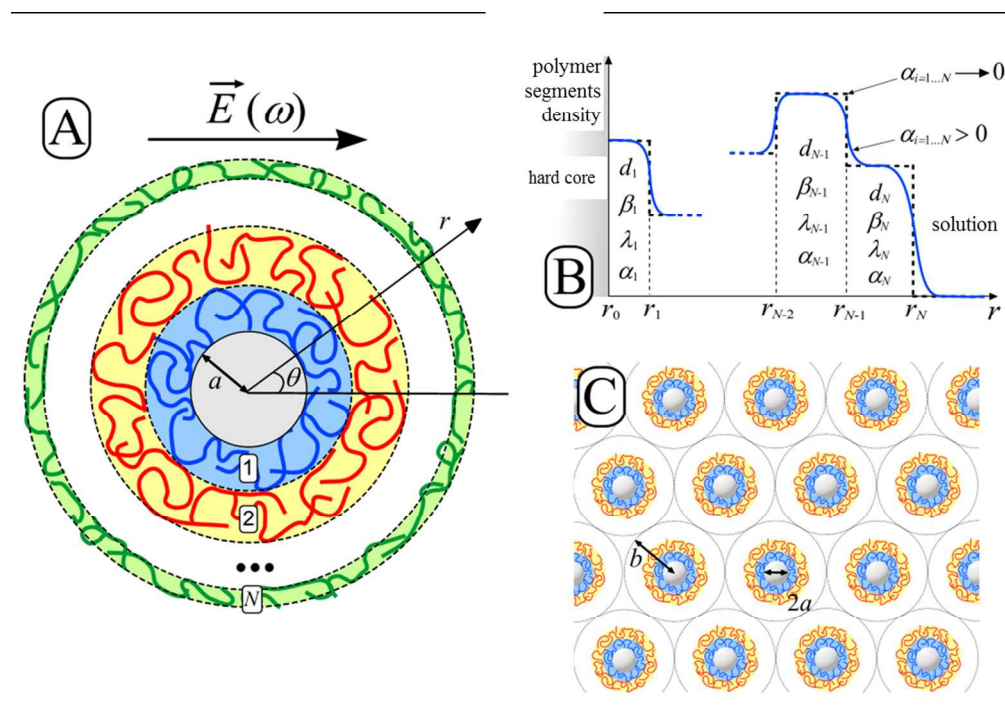
208x146mm (150 x 150 DPI)
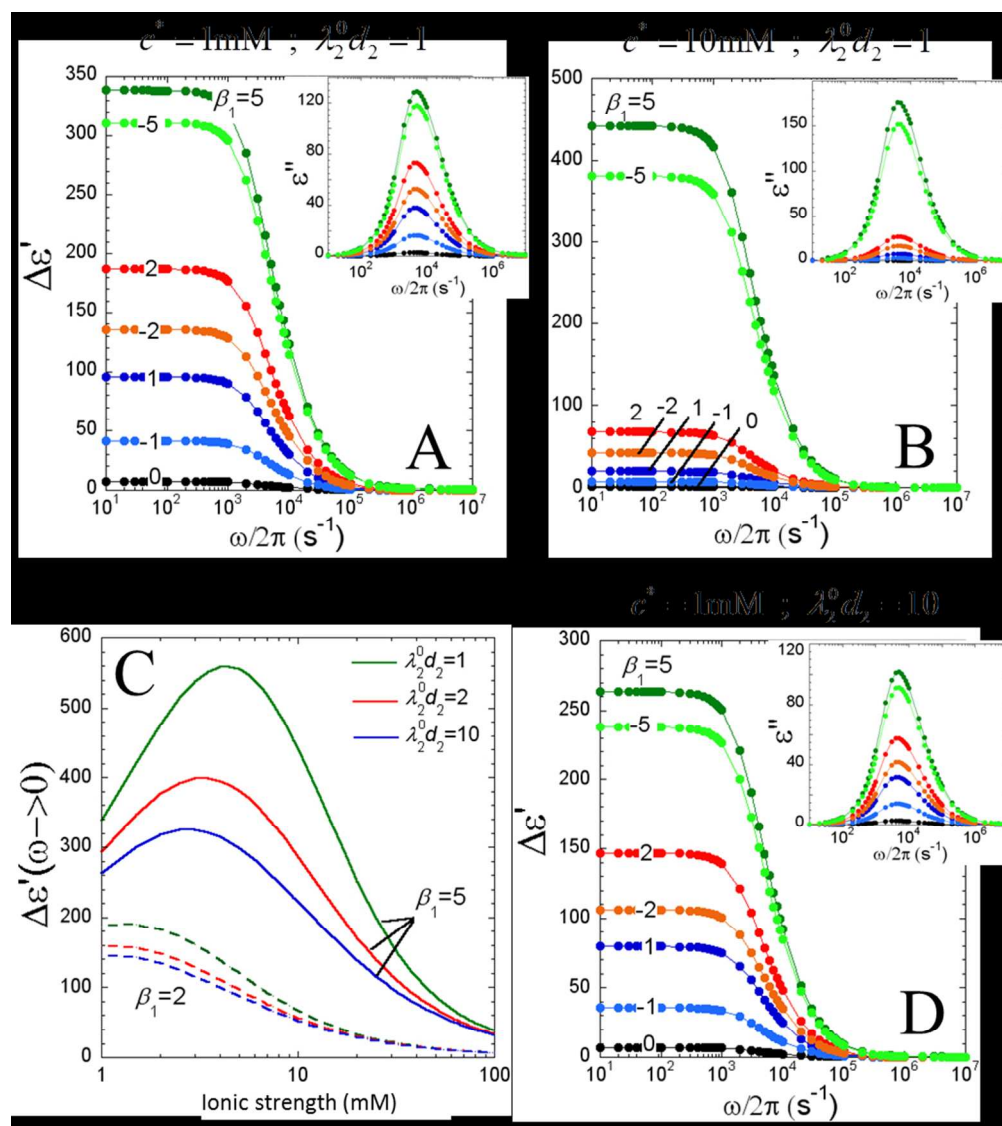
174x195mm (150 x 150 DPI)
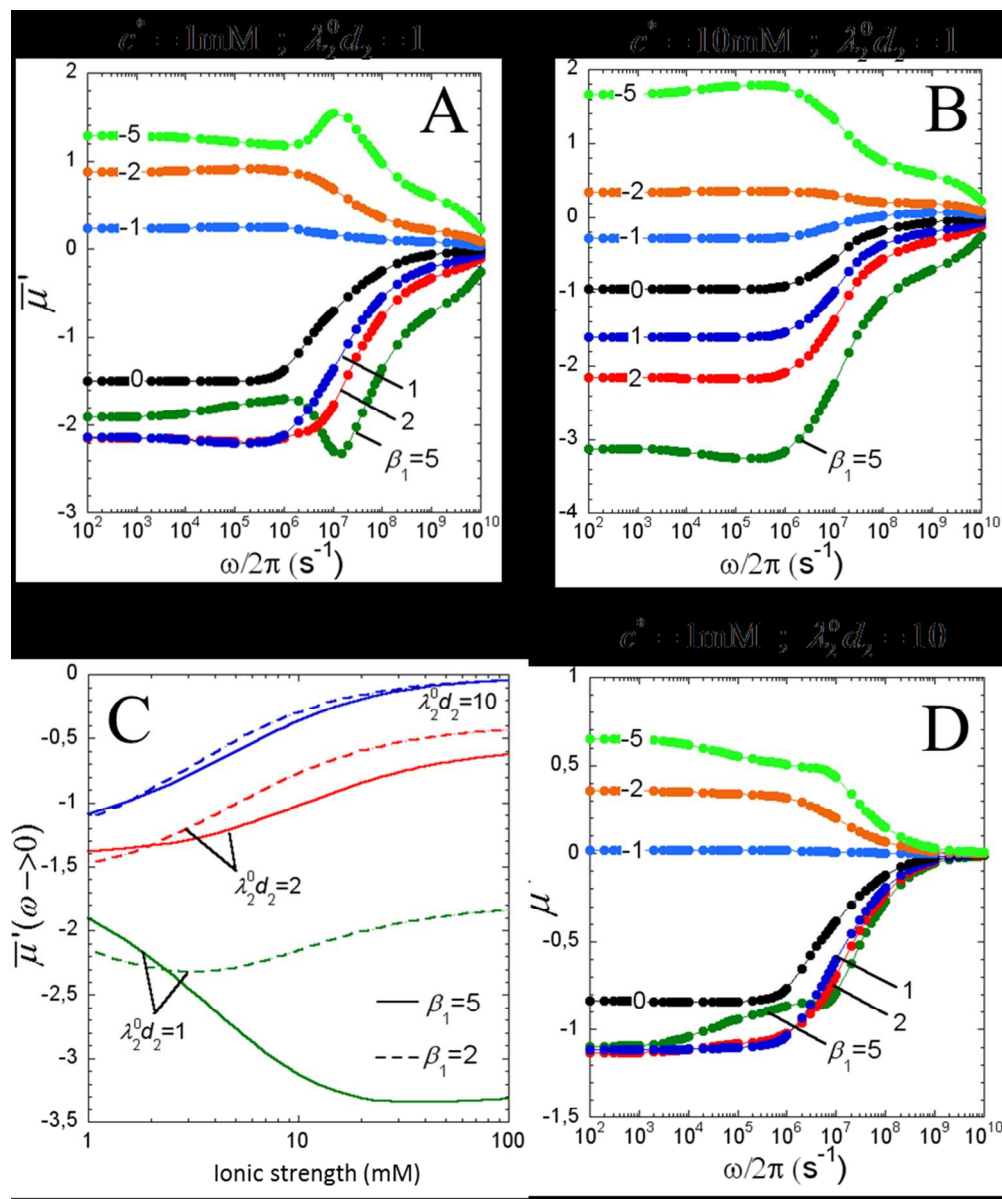
164x196mm (150 x 150 DPI)
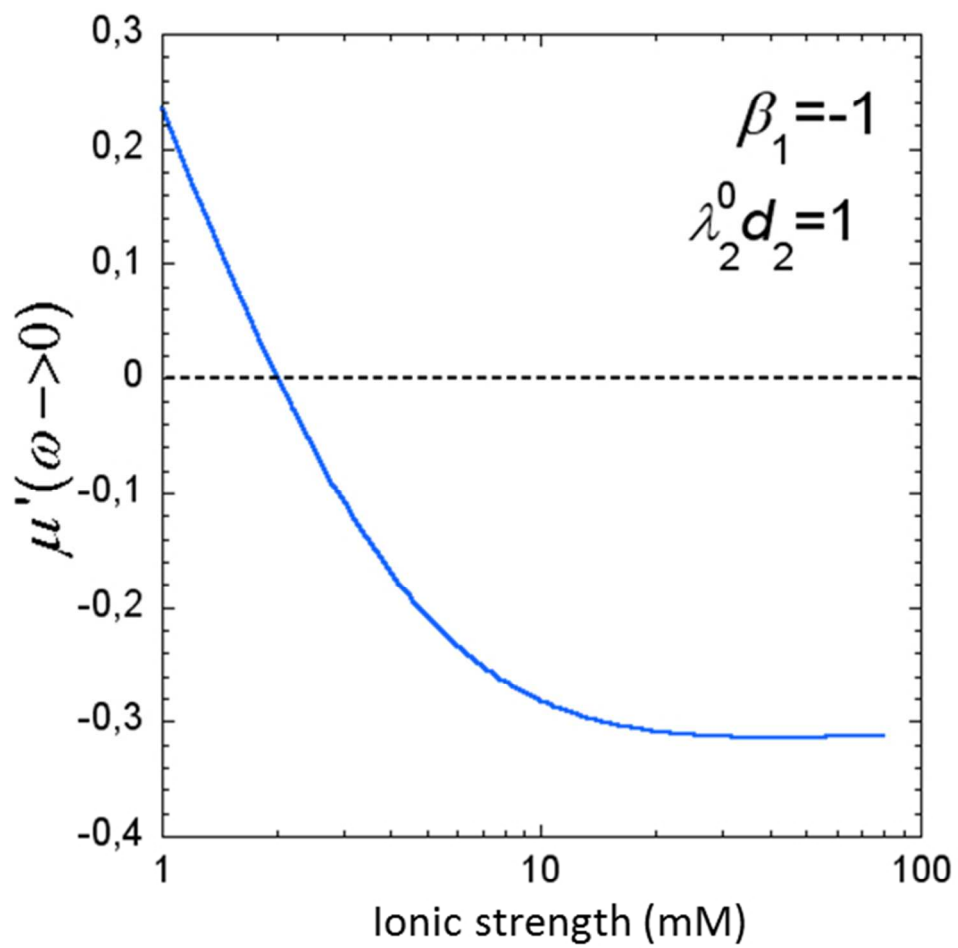
106x103mm (150 x 150 DPI)
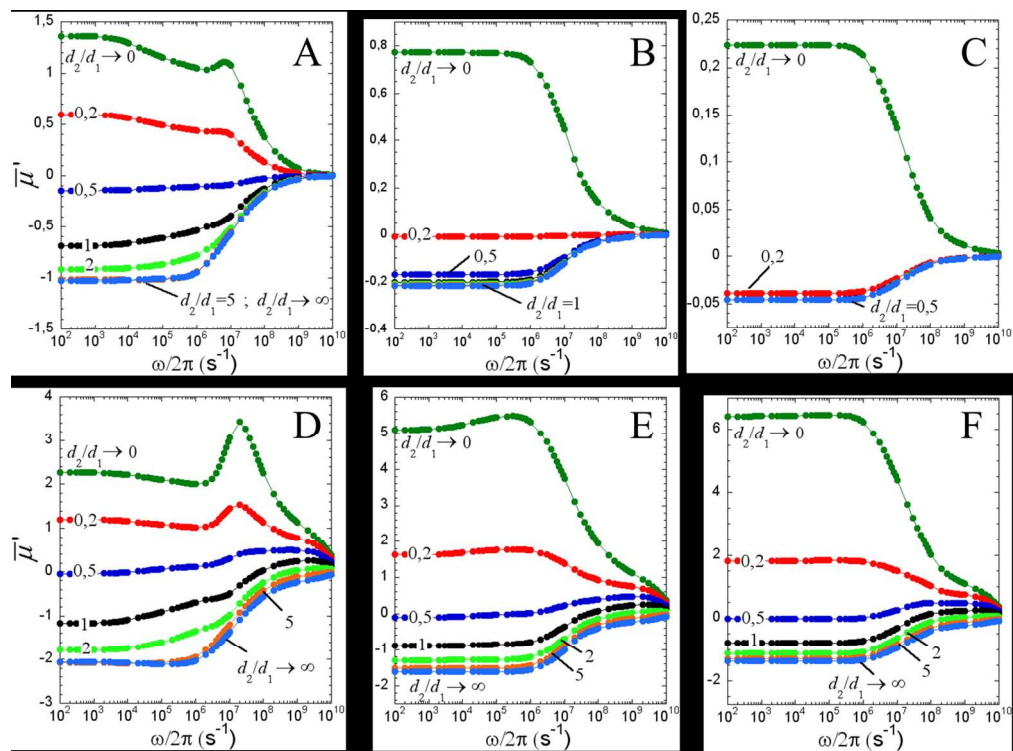
278x206mm (150 x 150 DPI)
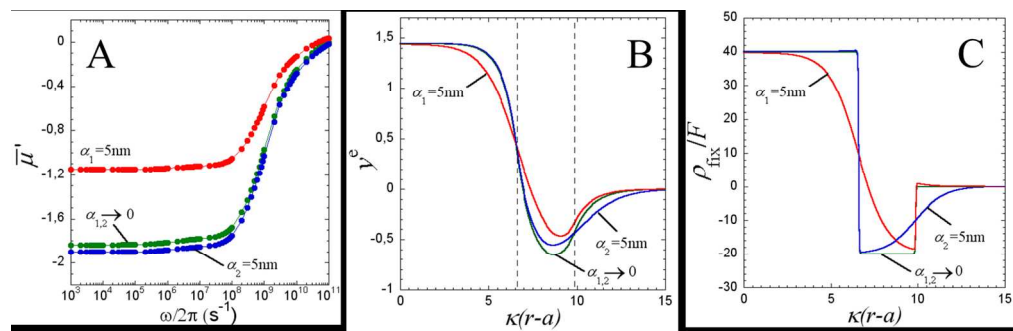
273x89mm (150 x 150 DPI)
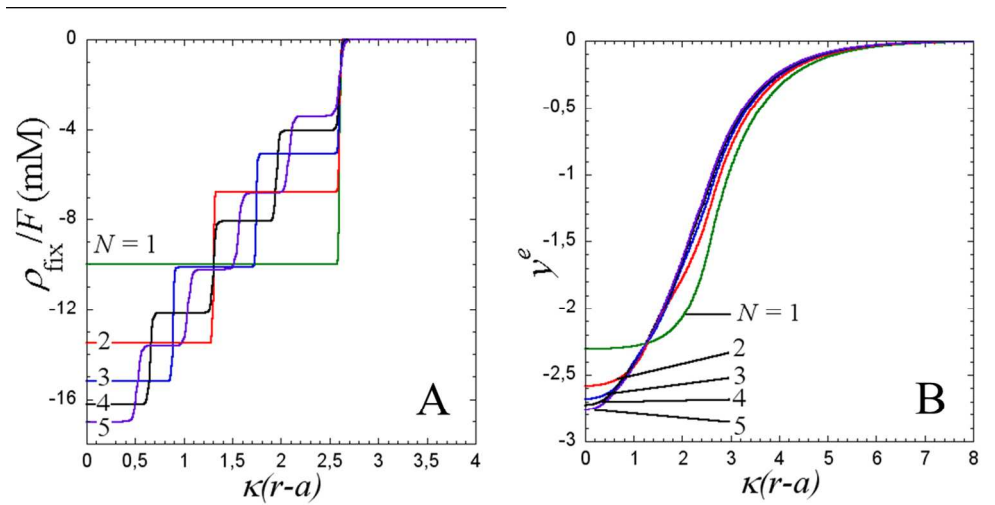
236x118mm (150 x 150 DPI)

197x205mm (150 x 150 DPI)